

## Answers to reviewer n°1

We first thank the reviewer for his helpful comments and suggestions that have helped us to improve the manuscript. In the following, we answer point by point using the following convention:

*The reviewer comments are in italic*

Our answers are in standard typo

The changes we made according to the recommendation of reviewer 1 of are in yellow in the track document.

*1. The introduction can be written in a much more accurate way. I would check it phrase by phrase and sentence by sentence.*

We rewrote the introduction taking into account the remarks of the reviewer

*1.1. Line 50-52 For example, one limitation of microscopy is the difficulty in indentifying picoplankton*

*1.2. The optical microscopy method is developing, for example the imaging flow cytometry (IFC).*

We rewrote these lines: “Microscopy is time-consuming and is unable to identify picoplankton. Imaging flow cytometry (IFC) has renewed microscopic methods, thanks to the speed at which they are able to characterize phytoplankton in a water sample (IOCCG report n°15, 2014)”. (Lines 49-52 in the revised version).

*1.3. Line 54-55: Mind the use of the terms PSC and PFT. PFT depends on how you define it. PSC is also a type of PFT definitions.*

Pigments allow estimating phytoplankton groups but not phytoplankton species. We withdrew this statement in the text.

*1.4. Line 57-60: the conversion formula method is the so-called "Diagnostic Pigment Analysis". CHEMTAX uses matrix factorization to estimate PFT from pigments.*

We mentioned the so-called “Diagnostic Pigment Analysis” line 57

*1.5. Line 60: I am not sure with just marker pigments themselves the identification of phytoplankton can be achieved in species level.*

We agree and we, therefore, modified the text of the revised version

*1.6. In summary, please check IOCCG report 15 and related literature carefully.*

According to comments n°3, 4, 5, 6 we rewrote these lines which are now (Lines 52-61 in the revised version) taking into account the material in the IOCCG report 15:

“An alternative method is the analysis of seawater samples by high-performance liquid chromatography (HPLC) which is widely used to categorize broad phytoplankton groups such as PFT or PSC (Jeffreys *et al*, 1997, Brewin *et al*, 2010, Hirata *et al*, 2011). HPLC enables identification of 25 to 50 pigments within a single analysis, which is much easier and faster to conduct than microscopic observations. Each phytoplankton group is associated with specific diagnostic pigments and a conversion formula can be derived to estimate the percentage of each group from the pigment measurements (Vidussi *et al*, 2001; Uitz *et al*, 2010). HPLC measurements are now recognized as the standard for calibrating and validating satellite-derived chlorophyll-a concentration and for mapping groups of phytoplankton (IOCCG report n°15, 2014)”.

*2. Lines 139-140 Match-up procedure can be more detailed, for example, by adding the criteria of refusing data points and the reason why you choose 20km*

We rewrote these lines in the revised version of the manuscript (lines 138-151)

“Matchup procedure between in situ and satellite observation is a crucial question to estimate remote sensing algorithms. If the parameters of the procedure are too severe, the number of collocated data is dramatically decreasing. If the parameters are too large, the accuracy of the matching is decreasing. We then chose some compromise. Usually, people use a matchup window of 3X3 pixels (Alvain et al, 2005) which corresponds to a distance somewhat less than 20km between the satellite pixel and in situ measurement since we deal with level 3 satellite observations whose pixel is of the order of 9X9km. This criterium refers to the typical length of ocean variability (Levy et al, 2012; Levy, 2003)”

*3. Lines 150-160 and Figure 3. Please use more statistical metrics in addition to R-square and RMSE according to Brewin et al 2015. Please specify whether they are calculated in log scale or not. Brewin, Robert JW, et al. "The Ocean Colour Climate Change Initiative: III. A round-robin comparison on in-water bio-optical algorithms." Remote Sensing of Environment 162 (2015): 271-294*

Brewin et al (2015) give a large variety of statistical parameters because they compare a large number of models whose performances are close together, which implies the use of several criteria to separate them. In the present study, we only need to estimate the quality of our model, which can be done by standard statistical parameters as usual.

Concerning the pigment concentrations, the statistical tests were done in  $\text{mg.m}^{-3}$ . We included this information in the text (lines 181-183).

In figure 3, we present the regression line between Chla- given by OC4V4 and in situ chl-a. The data are given in  $\text{mg.m}^{-3}$  and the statistical estimators were computed in  $\text{mg.m}^{-3}$  but the scale in figure 3 is log scales.

*4. Lines 288-289: you have said the same as Line 264-265.*

We insist on that point because it constitutes the original component of 2S-SOM.

*4. Table 2: often these statistics are done on log(pigments) - given their distribution and expected errors.*

Our strategy is to compute the statistical parameters in the physical space as most statisticians do and as did Brewin et al (2015) to facilitate the interpretation. The concentration values are normalized during the learning procedure of the SOM.

*5. Line 402: Unfortunately, it cannot be concluded that diatoms dominated because of high Fuco ratio and chl-a, without additional information on phytoplankton groups using e.g. microscopy.*

We do not have concomitant microscopy measurements. When analyzing the referent vectors presented in Fig 6, we strongly think that the bottom right region representing the neurons of the 2S-SOM may correspond to diatoms since high fucoxanthin is associated with high chlorophyll concentration and low peridinin. Besides, it is seen in Figures 8, 10 and 11 that high fucoxanthin geographical regions are situated near the coast where diatoms were observed in

previous studies (Farikou et al., 2015; Blasco et al., 1980) while high peridinin geographical regions are situated in offshore regions. We changed our previous sentence in:

‘Moreover, the bottom right region in the 2S-SOM may correspond to the diatoms with good confidence since high fucoxanthin is associated with high chlorophyll concentration and low peridinin. This is endorsed in section 5 by looking at the geographical location of the different pigment concentrations (figures 8, 10, 11)’. (Lines 352-356 of the revised version)

6. *Please spell MLP out in the Discussion section.*

MLP stands for Multi LayerPerceptron, it has been added on line 596

7. *Line 649-654: Can you summarize why SOM needs fewer data points than MLPs and other supervised learning? Why MLP cannot be trained with a total of ~500 data points?*

This is a well-known property of SOM versus MLP. The main difference between MLP and SOM is in the learning process: MLP is a supervised algorithm while SOM uses unsupervised learning. Both have to estimate a large number of weights during a learning phase; the accuracy of the methods depends on the dimension of the input and output spaces, the number of data available and the number of weights to estimate. In SOM the weights are highly regularized by the neighborhood function, so the number of data needed for learning is less than for the MLP. In the present application, the MLP would have to approximate a highly non-linear function from the R11 input space (the remote sensing parameters) to the R6 output space that represents the pigments. Due to the highly non-linearity of the function, the 515 data available for the learning is too small to adequately sample the R11 space of the function. On the other hand, SOM is not a regressor but uses automatic clustering methods and provides more robust values. Moreover, the topological order prevents to make errors in interpolating between two clusters. We think this explanation is too long to be included in the present text and out of the scope of the present study. It would be relevant in a Text Book or a review paper dedicated to NN. We propose to escape this question and to withdraw the sentence at line 650: ‘which makes MLPs and classical supervised learning methods unusable’ The sentence is now:

‘We used an unsupervised neural network classification method which is an extension of the SOM method well adapted to deal with a small database whose elements are very inhomogeneous’(lines 605-607 of the revised version)

8. *Is it possible to clarify the minimum threshold of pigment concentration of the applicability of 2S-SOM?*

The minimum and maximum values of a parameter are those of the learning data base. As the 2S-SOM has 162 neurons, the interval between the minimum and maximum values is divided into 162 discrete values corresponding to the values captured by the referent vector associated with each neuron. Classification acts as a piecewise continuous model permitting the achievement of complex tasks. We get these discrete values empirically only by looking at the different referent vectors of the SOM.

## TECHNICAL CORRECTIONS

1. *The country Senegal has three versions of names in the manuscript, i.e. Sel̃ Anel̃ Agalo (title), Senegalo (context) and Senegal (Figure 1). Please keep the consistency.*

We homogenized the spelling of Senegal in the revised version

2. *line 41 The word “phytoplankton” is more often used as a plural*  
modified (line40, 41, 49 of the revised version)

3. Line 42-44: mind the subscript of CO<sub>2</sub>  
modified

4. lines 43-44: I have not found the information of 30% in Behrenfield et al, 2005  
We put a more appropriate reference for the rate of CO<sub>2</sub> captured by the ocean: “Le Quéré et al, 2018” (line 43)

5. line 48: The description "fish grazing on phytoplankton" is not accurate. The effect of phytoplankton on fisheries is via marine food chain, i.e. zooplankton grazing on phytoplankton provide food source for some fish.

We changed the sentence as: “and fisheries with a possible effect on fish grazing on phytoplankton via the marine food chain” (line 46-47 of the revised version)

6. Line 56: Please add the citation: Sosik, H.M.; Sathyendranath, S.; Uitz, J.; Bouman, H.; Nair, A. In situ methods of measuring phytoplankton functional types. In *Phytoplankton Functional Types from Space. Reports of the International Ocean-Colour Coordinating Group (IOCCG), No. 15*; Sathyendranath, S., Ed.; IOCCG: Dartmouth, NS, Canada, 2014; pp. 21–38  
Done (line 56 in the revised version)

7. Line 84: use the abbreviation of "PSC". Full name is not needed  
Done

8. line 86: the term "PSC percentage" is inaccurate. It is the contributions of Chl<sub>a</sub> from different phytoplankton size classes to total Chl<sub>a</sub> concentration

We modified the sentence as: ‘ These algorithms try to establish a relationship between the chl-a concentration and the chl-a concentration fractions associated with each of the three PSC’ (lines 86-88 of the revised version)

9. Line 105: the colour of the land is not red.  
We changed ‘red’ into ‘brown

10. Line 111: delete "a".

11. Line 112: "systems".

12. Line 161: "wavelengths".

13. Please define the abbreviation of a variable before using it (e.g. Table 1 and a lot of places).  
We implemented the suggested corrections.

14. lines 181-182: this not a sentence

We modified this line which is now ‘which is defined as the ratio of the diagnostic pigment (DP) versus the total chl-a’. (lines 178-179 of the revised version)

15. Line 182: typo: divinyl chl-a. Did you consider chlorophyllide-a as part of Tchl-a?

We used the definition of Alvain et al (2005), where Chl-a is part of Tchl-a (Tchl-a= Chl-a+ Divinyl chlorophyll-a). (line 179)

16. Line 186-190: you have mentioned these in Line 113-117

We delete the sentence in lines 186-190

17. Figure 4&5: *Rrs* is not defined.

*Rrs* stands for  $\rho_w(\lambda)$ , we made the change in figures 4 and 5 in the revised version

The manuscript has been read and corrected by a native English-speaking person

#### **Added references**

Levy, M., Mesoscale variability of phytoplankton and of new production: Impact of the large-scale nutrient distribution, J. Geophys. Res., 108(C11), 3358, doi:10.1029/2002JC001577, 2003.

M. Lévy, D. Iovino, L. Resplandy, P. Klein, G. Madec, A.-M. Tréguier, S. Masson, K. Takahashi, (2012) Large-scale impacts of submesoscale dynamics on phytoplankton: Local and remote effects, *Ocean Modelling*, 77–93

Le Quéré et al, (2018) *Global Carbon Budget 2018*, *Earth Syst. Sci. Data*, 10, 2141–2194, 2018 ; <https://doi.org/10.5194/essd-10-2141-2018>

Sosik, H.M.; Sathyendranath, S.; Uitz, J.; Bouman, H.; Nair, A. In situ methods of measuring phytoplankton functional types. In *Phytoplankton Functional Types from Space*. IOCCG report, No. 15; Sathyendranath, S., Ed.; IOCCG: Dartmouth, NS, Canada, pp. 21–38, 2014.

## Answers to reviewer n°2

We first thank the reviewer for his helpful comments and suggestions that have helped us to improve the manuscript. In the following, we answer point by point using the following convention:

*The reviewer comments are in italic*

Our answers are in standard typo

The changes we made according to the recommendation of reviewer 2 of are **in turquoise** in the track document

*There is a lack of comparison with controls for the reader to appreciate the advantage of using this new model. At the minimum, there should be more comparison between the new 2S-SOM model performance scores versus the standard SOM model scores. [The paper would be more interesting if the performance of 2S-SOM is also compared against standard supervised learning models such as multi-layer perceptrons or random forests.]*

We comment on the advantages/disadvantages of the different methods in the discussion section (line 594-609 of the revised version). An objective comparison of the different methods is out of the scope of the present paper as it would considerably increase the length of the present paper. In fact, it would deserve a full paper (see the paper of Brewin et al (2011) dedicated to a comparison of the different methods and also the paper of Bracher et al, 2017, Obtaining Phytoplankton Diversity from Ocean Color: A Scientific Roadmap for Future Development. Front. Mar. Sci. 4:55.). Besides to be conclusive, such a comparison should be done on a specific region where in situ measurements are more numerous than in the present region. We first used a SOM and then decided to use a 2S-SOM mainly by the information provided by the 2S-SOM on the role of the different variables in the classification process. The major advantage of the 2S-SOM compared with the SOM and other classification methods is to partition the different variables of the dataset under study into blocks and to affect weights to these blocks. The block weighting facilitates the clustering procedure by favoring the taking into account of the most pertinent variables. This method is related to the research area developed in statistics under the designation of clusterwise method (Parson et al 2004; Kriegel et al 2009)

Parsons L, Haque E et Liu H : Subspace clustering for high dimensional data : a review. SIGKDD Explor. Newsl., pages 90105, 2004. ISSN 1931-0145. 73, 74, 80  
Kriegel H.-P, Kröger P et Zimek A : Clustering high-dimensional data : A survey on subspace clustering, pattern-based clustering, and correlation clustering. ACM Trans. Knowl. Discov. Data, 3(1):1 :11 :58, mars 2009. ISSN 1556-4681. 37, 73, 74, 80

A high weight affected to a block means that the associated variables play a major role in the classification process; a small value means that the associated variable plays a minor role: this information is of importance to identify the variables which control the process under study. Besides the block weighting provides useful information on the functioning of the classification by permitting to identify the variables which control it and allows us to better understand the dynamics of the phytoplankton communities. This is discussed in lines 371-376 of section 4-2 **Analysis of the topology of the 2S-SOM** corresponding to the analysis of figure 7 showing the different weights affected to the neurons of the 2S-SOM also in lines 494-509 of section 5 corresponding to the analysis of figure 13, and in line 622-627 of the discussion section. Moreover, we added the block weights  $\alpha$  as an output of 2S-SOM in figures 4 and 5



*On line 321, the choice of the elongated 2-dimensional grid of 9x18 is not obvious. Why is a more square grid (e.g. 12x12, 12x13 or 13x13) not used?*

The size of the map has been determined (line 275-276, added in the new version), by using the SOM software

<http://www.cis.hut.fi/projects/somtoolbox/download/>, assuming that the size of SOM and 2S-SOM depend on the same criteria. We also checked other grid configuration and found that the most efficient is the 9x18 neurons

*The paper is very hard to read as there is a tendency to present many undefined symbols all at once, with the symbols remaining undefined until much later in the paper. For instance, Eq.(5) introduces a large number of symbols and terms all at once. The “block” is not explained in a concrete way until the next section (Sect. 3.3), so I had a misconception on how the data were blocked when reading Sect. 3.2. A much more logical order of presentation is to present the concept of blocking variables first, and try to explain as many of the symbols coming up in Eq.(5) before actually presenting the equation. Also around Eq.(5), there are numerous typos and inconsistent fonts (as listed later in this review).*

We have rewritten the sections 3.1 and 3.2 describing the functioning of the SOM and 2S-SOM. We put in Annex the mathematical description of that functioning. In the main text, we only describe the principle of the functioning of the 2S-SOM.

We now explain all the symbols we used. The blocks are described in the main text (lines 255-260) before the explanation of the functioning of the SOM and the 2S-SOM, which is in Annex. We also focused attention on the typos

*Line 22-23 Thanks to . . . new method. It primarily consists in. . .” is verbose. Simplify to “Our new method consists of.*  
done (line 22)

*Line 25 “carried using” should be “carried out using”.*  
done (line 24)

*Line 69 and throughout the manuscript: Bold fonts are for vectors and matrices (see the journal’s manuscript preparation guidelines), but here they are often used for scalars and units. There are many places where the font switches back and forth between bold and Roman and italics (e.g. lines 248-251 and line 272).*

We carefully read the manuscript and corrected the font errors

*Line 151: Need a reference for the OC4V4 algorithm.*

We give a reference for the OC4V4 algorithm (O’Reilly et al, 2001) – (line 154 in the revised version)

*Line 162 The last sentence of the paragraph and Table 1 need to be moved to after line 183. The table is currently placed before the terms in it are defined.*

Done

*Line 174: How can Ra be independent of chl-a if it is divided by rho\_wref which is dependent on chl-a?*

Ra, which is defined as  $\rho_W(\lambda) / \rho_{WREF}(\lambda, chl-a)$  is the key parameter of the Physat method (Alvain et al, 2005, 2012).  $\rho_W(\lambda)$  depends on secondary phytoplankton pigments + chl-a, while  $\rho_{WREF}(\lambda, chl-a)$  depends on chl-a only. The reasoning of Alvain et al (2005) is that the ratio  $\rho_W(\lambda) / \rho_{WREF}(\lambda, chl-a)$  depends on secondary phytoplankton only since both depend on chl-a.

*Line 248: W is undefined.*

W is now defined in line 230

*Line 254: should give a specific reference on the kernel and temperature.*

References are given in lines 930, 931 of Annex (Kohonen, 2001, Niang et al, 2003)

*Line 276: How were B and Pb chosen?*

These variables are defined in lines 941 and 944: B is the number of blocks (B=4) and Pb is the number of variables in block b. According to the definition of blocks (lines 257-262), P1= 5, P2= 5, P3= 5, P4= 2.

*Line 278: “a” should be alpha.*

Corrected (line 953 in the new version)

*Line 282: Eta should be beta.*

Corrected (line 953 in the new version)

*Figure 4: For 2S-SOM, I can see long dash, short dash, space and no space variants.*

Figure 4. We check the pdf output corresponding the figure 4. It seems ok in the modified version. Perhaps there was a software problem in the conversion of the original text written in Word into pdf.

*Line 420: Last sentence of paragraph: I have trouble understanding this sentence.*

We changed this sentence and gave more explanation on the description of the 2S-SOM neurons. The sentence is now (Line 381-384 in the new version):

“These neurons correspond to very small *chl-a* concentrations, which are estimated with large errors. Besides, we remark that high  $\alpha$  values for *chl-a* correspond to high *chl-a* concentration values (bottom right of the *chl-a* panel in figure 7 and figure 6 respectively). For these cases, the clustering assembled data that mainly depend on *chl-a* concentration”.

*Fig.13: Top right corner is slightly chopped off.*

Done.

*Line 542: “a” should be alpha.*

Done. We replaced ‘a weight’ by ‘a weight  $\alpha$ ’ which is clearer (line 497 of the new version)

*Fig.16: I don’t understand why the black curve tends to lie closer to the blue curve than the red curve is to the blue curve. I would have expected the red curve to lie closer to the blue curve. I might have misunderstood what the curves represent – please give more detailed explanation.*

A VIIRS sensor observation is captured by a neuron of the 2S-SOM whose associated referent spectrum is the red curve in figure 16. This referent spectrum is the mean of the different spectra captured by that neuron during the learning phase. Among these different spectra, there is one (black curve in figure 16) which is the closest to the UPSEN spectrum (blue curve in figure 16).



It is expected that the black curve is closer to the blue curve than the red curve which is flattened due to the averaging process. We reformulated this description in the text which was not clear in the first version. (line 539-546).

*Line 639: Replace “people” with “studies”.*

Done (line 596 of the revised version).

REVISED DOCUMENT  
With changes

MS No.: os-2019-11

The changes suggested by reviewer 1 are in yellow

The changes suggested by reviewer 2 are in turquoise

**ESTIMATION OF PHYTOPLANKTON PIGMENTS FROM OCEAN-COLOR  
SATELLITE OBSERVATIONS IN THE SENEGALO-MAURITANIAN REGION BY  
USING AN ADVANCED NEURAL CLASSIFIER**

By

Khalil Yala<sup>1</sup>, N'Dye Niang<sup>2</sup>, Julien Brajard<sup>1,4</sup>, Carlos Mejia<sup>1</sup>, Maurice Ouattara<sup>2</sup>, Roy El  
Hourany<sup>1</sup>, Michel Crépon<sup>1</sup> and Sylvie Thiria<sup>1,3</sup>

<sup>1</sup> IPSL/LOCEAN, Sorbonne Université (Université Paris6, CNRS, IRD, MNHN), 4 Place  
Jussieu, 75005 Paris, France

<sup>2</sup> CEDRIC, CNAM, 292 rue Saint Martin, 75003 Paris, France

<sup>3</sup> UVSQ, F-78035, Versailles, France

<sup>4</sup> Nansen Center, Thormøhlensgate 47, 5006, Bergen, Norway

Corresponding author: Michel Crepon ([crepon@locean-ipsl.upmc.fr](mailto:crepon@locean-ipsl.upmc.fr))

**ABSTRACT**

We processed daily ocean-color satellite observations to construct a monthly climatology of phytoplankton pigment concentrations in the Senegalo-Mauritanian region. Thanks to the difficulty of the problem, we proposed a new method. **Our new method** primarily consists in associating, in well-identified clusters, similar pixels in terms of ocean-color parameters and in situ pigment concentrations taken from a global ocean database. The association **is carried out** using a new Self Organized Map (2S-SOM). Its major advantage is to allow taking into account the specificity of the optical properties of the water by adding specific weights to the different ocean color parameters and the in situ measurements. In the retrieval phase, the pigment concentration of a pixel is estimated by taking the pigment concentration values associated with the 2S-SOM cluster presenting the ocean-color satellite spectral measurements, which are the closest to those of the pixel under study according to some distance. The method was validated by using a cross-validation procedure. We focused our study on the fucoxanthin concentration, which is related to the abundance of diatoms. We showed that the fucoxanthin starts to develop in December, presents its maximum intensity in March when the upwelling intensity is maximum, extends up to the coast of Guinea in April and begins to decrease in

May. The results are in agreement with previous observations and recent in situ measurements. The method is very general and can be applied in every oceanic region.

## 1 - INTRODUCTION

Phytoplankton are the basis of the ocean food web and consequently drive the ocean productivity. They also play a fundamental role in climate regulation by trapping atmospheric carbon dioxide (CO<sub>2</sub>) through gas exchanges at the sea surface, and consequently lowering the rate of anthropogenic increase in the atmosphere of CO<sub>2</sub> concentration by about 25% (*Le Quéré et al, 2018*). With the growing interest in climate change, one may ask how the different phytoplankton populations will respond to changes in ocean characteristics (temperature, salinity, acidity) and nutrient supply, which presents an important societal impact with respect to both climate and fisheries, with a possible effect on fish grazing phytoplankton via the marine food chain.

Methods for identifying phytoplankton have greatly progressed during the last two decades. Phytoplankton were first described by microscopy. Microscopy is time consuming and is unable to identify picoplankton. Imaging flow cytometry (IFC) has renewed microscopic methods, thanks to the speed at which they are able to characterize phytoplankton in a water sample (IOCCG report n°15, 2014). An alternative method is the analysis of seawater samples by high-performance liquid chromatography (HPLC) which is widely used to categorize broad phytoplankton groups such as PFT or PSC (*Jeffreys et al, 1997, Brewin et al, 2010, Hirata et al, 2011*). HPLC enables the identification of 25 to 50 pigments within a single analysis, which is much easier and faster to conduct than microscopic observations (*Sosik, H.M et al, 2014*). Each phytoplankton group is associated with specific diagnostic pigments, and a conversion formula, the so-called “Diagnostic Pigment Analysis” can be derived to estimate the percentage of each group from the pigment measurements (*Vidussi et al, 2001; Uitz et al, 2010*). HPLC measurements are now recognized as the standard for calibrating and validating satellite-derived chlorophyll-a concentration and for mapping groups of phytoplankton (IOCCG report n°15, 2014).

The use of satellite ocean color sensor measurements has permitted to map the ocean surface at a daily frequency. Satellite sensors measure the sunlight, at several wavelengths, backscattered by the ocean. The downwelling sunlight interacts with the seawater through backscattering and absorption in such a manner that the upwelling radiation transmitted to the satellite (‘water-leaving’ reflectance) contains information related to the composition of the seawater. The light transmitted to the satellite depends

on the phytoplankton cell shape (backscattering), its pigments (absorption), the dissolved matter (e.g. CDOM).

This upwelling radiation, the so-called remotely sensed reflectance  $\rho_w(\lambda)$ , is determined by the spectral absorption  $a$  and backscattering ( $b_b(\text{m}^{-1})$ ) coefficients of the ocean (pure water and various particulate and dissolved matters) using the simplified formulation (Morel and Gentili, 1996):

$$\rho_w(\lambda) = G \frac{b_b(\lambda)}{a(\lambda) + b_b(\lambda)} \quad (1)$$

where  $a(\text{m}^{-1})$  is the sum of the individual absorption coefficients of water, phytoplankton pigments, colored dissolved organic matter, and detrital particles,  $b_b(\text{m}^{-1})$  depends on the shape of the phytoplankton species.  $G$  is a parameter mainly related to the geometry of the situation (sensor and solar angles) but also to environmental parameters (wind, aerosols).

In the open ocean far from the coast (in case-1 waters), the light seen by the satellite sensor mainly contains information on phytoplankton abundance and diversity. Ocean-color measurements have been first used intensively to estimate chlorophyll-*a* concentration (*chl-a* in the following) in the surface waters of the ocean, marginal seas and lakes. (Longhurst *et al.*, 1995; Antoine *et al.*, 1996; Behrenfeld and Falkowski, 1997; Behrenfeld *et al.*, 2005; Westberry *et al.*, 2008).

It has been shown that it is also possible to extract additional information such as phytoplankton size-classes (PSC) by using some relationship between chlorophyll concentration and PSC (Uitz *et al.*, 2006; Ciotti and Bricaud, 2006; Hirata *et al.*, 2008; Mow and Yoder, 2010). These algorithms try to establish a relationship between the *chl-a* concentration and the *chl-a* concentration fractions associated with each of the three PSC. Some of them (Uitz *et al.*, 2006; Aiken *et al.*, 2009) break-down the *chl-a* abundance into several ranges for each of which a specific relationship is computed. Others (Brewin *et al.*, 2010; Hirata *et al.*, 2011) are based on a continuum of *chl-a* abundance. Studies have also been done to estimate the phytoplankton groups (PFT) by taking into account spectral information (Sathyendranath *et al.*, 2004, Alvain *et al.*, 2005, 2012; Hirata *et al.*, 2011; Ben Mustapha *et al.*, 2013; Farikou *et al.*, 2015). This is of fundamental interest to the understanding of the phytoplankton behavior and to modeling its evolution.

Due to highly non-linear relationship linking the multispectral ocean color measurements with the pigment concentrations, we proposed a neural network clustering algorithm (2S-SOM) able to deal with multi variables linked by complex relationships. The 2S-SOM algorithm is well adapted to this complex task by weighting the different inputs. The clustering algorithm was calibrated on a restricted database composed of remote sensed observations co-located with measurements taken in the global ocean.

In the present paper, we propose the retrieval of the major pigment concentrations from satellite ocean color multi-spectral sensors in the Senegalo-Mauritanian upwelling, which is an oceanic region off the coast of West Africa where a strong seasonal upwelling occurs (Figure 1).

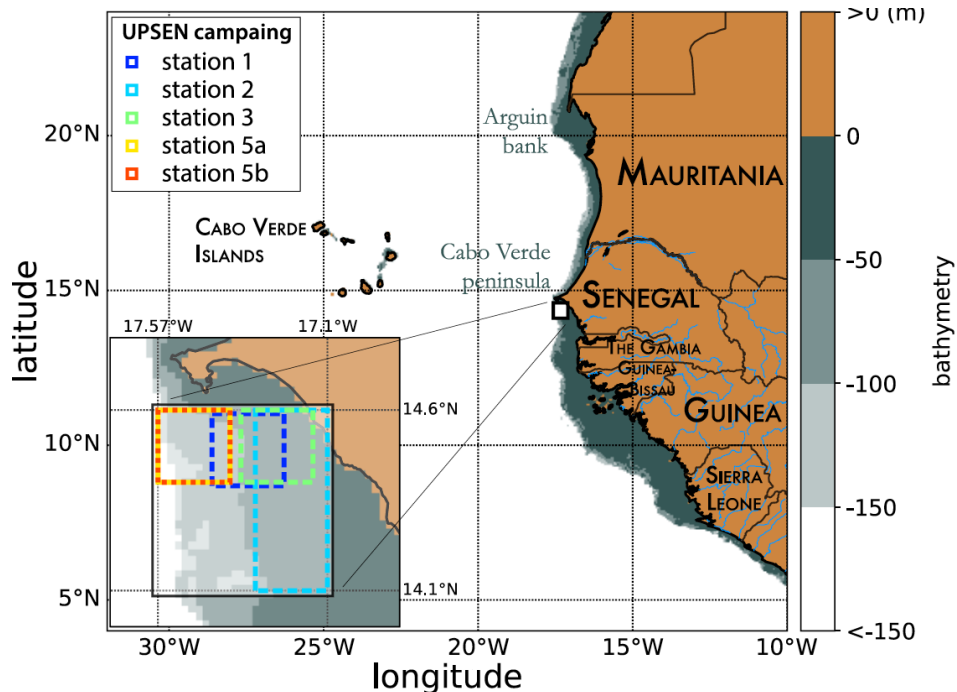


Figure 1: Mauritania and Senegal coastal topography. The land is in brown and the ocean depth is represented in meters by the color scale on the right side of the figure. The UPSEN stations are shown at the bottom left cartoon of the figure.

The Senegalo-Mauritanian upwelling is one of the most productive eastern boundary upwelling systems (EBUS) with strong economic impacts on fisheries in Senegal and Mauritania. Since the region has been poorly surveyed in situ, we have chosen to extract pertinent biological information from ocean-color satellite measurements. The region has been intensively studied by analysis of SeaWiFS ocean-color data and AVHRR sea-surface temperature as reported in Demarcq and Faure (2002), Sawadogo et al. (2009), Farikou et al. (2013, 2015), Ndoye et al. (2014) and more recently by Capet et al. (2017) with in situ observations.

The paper is articulated as follows: in section 2, we present the data we used (in situ and remote sensing observations). The mathematical aspect of the clustering method (2S-SOM) is detailed in section 3. In section 4 we present the methodological results. The spatio-temporal variability of the fucoxanthin and chl-a concentration in the Senegalo-Mauritanian upwelling region are presented in section 5, as well as the results of the oceanic UPSEN campaigns. In section 6 we discuss the results and the method. A conclusion is presented in section 7.

## 2- MATERIALS

In this study we used three distinct datasets: the first was used to calibrate the method, the second to conduct a climatological analysis of the Senegalo-Mauritanian upwelling region and the third was obtained during the oceanographic UPSEN campaign. These datasets are composed of satellite remote sensing observations and in-situ measurements.

### 2.1 The calibration data base (DPIG)

The calibration database (DPIG) comprises in situ pigment measurements co-located with satellite ocean-color observations done by the SeaWiFS (Sea-viewing, Wide-Field-of-view Sensor).

This DPIG is composed of 515 matched satellite observations and in situ measurements made in the global ocean (mainly in the North Atlantic and the equatorial ocean; *Ben Mustapha et al.*, 2014). The match-up criteria were quite severe: we used satellite pixel situated at a distance less than 20km from the in situ measurement in a time window of +/- 12h. The geographic distribution of the 515 coincident in situ and satellite measurements is shown in Fig. 2.

Matchup procedure between in situ and satellite observation is a crucial question to estimate remote sensing algorithms. If the parameters of the procedure are too severe, the number of collocated data is

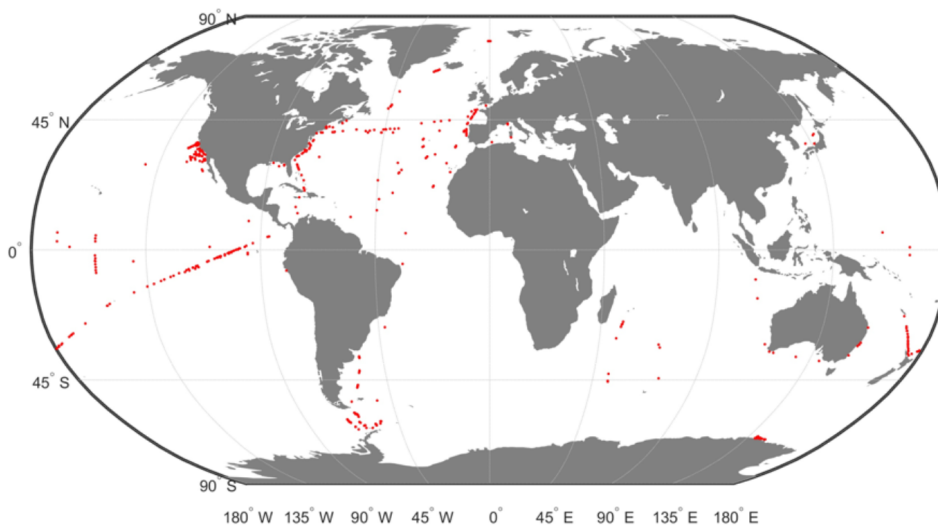


Figure 2: Geographic positions of the 515 in situ and satellite collocated measurements of the DPIG database.

dramatically decreasing. If the parameters are too large, it is the accuracy of the matching, which is decreasing. We accordingly chose some compromise. Usually people use a matchup window of 3X3 pixels



(Alvain et al, 2005) which corresponds to a distance less than 20km between the satellite pixel and in situ measurement, since we deal with level 3 satellite observations whose pixel is of the order of 9X9km. This criterium refers to the typical length of ocean variability (Levy et al, 2012; Levy, 2003)

In Figure 3 we present the  $R^2$  coefficient between the in situ *chl-a* and the SeaWiFS *chl-a* computed by using the OC4V4 algorithm (O'Reilly et al, 2001) for the DPIG collocated observations. We remark that the two measurements are in good agreement at global scale. Each data of DPIG is a vector

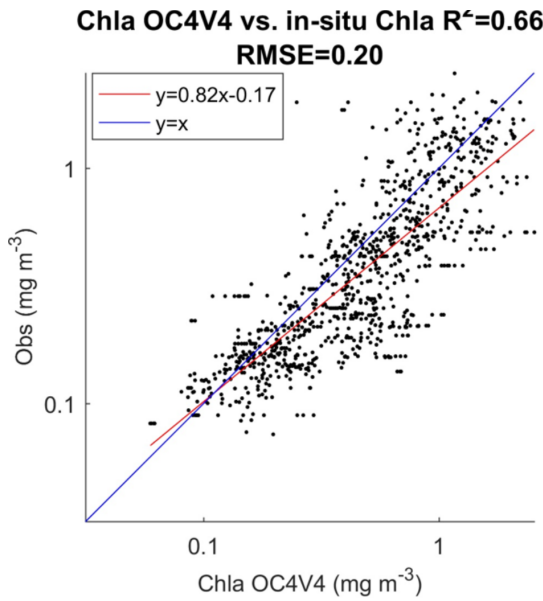


Figure 3: Dispersion diagram of DPIG *chl-a* computed from the SeaWiFS observations using the OC4V4 algorithm versus in situ *chl-a*. The coefficient of vraisemblance  $R^2$  and the RMSE (Root Mean Square Error) were computed in in  $\text{mg m}^{-3}$

having 17 components (five ocean reflectance ( $\rho_w(\lambda)$  and  $Ra(\lambda)$  at five wavelengths (412, 443, 490, 510 and 555nm), SeaWiFS *chl-a*, five in situ pigment ratios and in situ *chl-a* concentration). The in situ *chl-a* concentration ranges between 0.007 and 3.  $\text{mg m}^{-3}$  (see Table 1).

The five  $Ra(\lambda)$  are defined following Alvain et al, (2012 :

$$Ra(\lambda) = \rho_w(\lambda) / \rho_{wref}(\lambda, chl-a) \quad (2)$$

where the parameter  $\rho_{wref}(\lambda, chl_a)$  is an average reflectance depending on the *chl-a* concentration only which was computed according to the procedure reported in Farikou et al, 2015.  $Ra(\lambda)$  is a non-

dimensional parameter which is independent of the *chl-a* abundance and sensitive to the secondary pigments only (Alvain *et al* , 2012).

The DPIG database thus provides information on the existing links between the pigment composition and the SeaWiFS measurements. The pigment composition are defined by the pigment ratios which are non-dimensional variables of the form in the present study:

$$\text{Pigment Ratio} = \text{DP} / \text{Tchl-a} \quad (3)$$

which is defined as the ratio of the diagnostic pigment (DP) versus the total *chl-a* ( $\text{Tchl-a} = \text{chl-a} + \text{divinyl chl-a}$ , according to Alvain *et al.*, 2005).

The pigments of the DPIG and their statistical characteristics are given in Table 1. The statistical tests presented in Figure 3 ( $R^2$  and RMSE) and in Table 1 (MEAN, STD, MIN, MAX) were computed in  $\text{mg m}^{-3}$ .

	RDIVINY A	RPERID	RFUCO	R19HF	RZEAX	CHLORO IN SITU
MEAN	0.1414	0.0272	0.1248	0.1859	0.1696	0.5292
STD	0.1584	0.0196	0.0971	0.0996	0.2063	0.5720
MIN	0.0037	0.0035	0.0053	0.0066	0.0027	0.007
MAX	0.8889	0.2027	0.8514	0.7654	1.5574	2.9980

Table 1: *Pigments of the DPIG and their statistical characteristics: :STD (Standard Deviation), MIN (minimum value), MAX (maximum value).*

## 2.2 The Senegalo-Mauritanian upwelling satellite data (DSAT)

The satellite dataset we processed to retrieve the pigment concentration consist of five  $\rho_w(\lambda)$  and five  $Ra(\lambda)$  at five wavelengths (412, 443, 490, 510 and 555nm), and the SeaWiFS *chl-a* concentration observed in the Senegalo-Mauritanian upwelling region (8°N-24°N, 14°W-20°W; Figure 3) during 11 years (1998-2009) by SeaWiFS. This data set is here below denoted *DSAT*.

The satellite observations ( $\rho_w(\lambda)$  and *chl-a* concentration) were provided by NASA with a resolution of nine kilometers. Due to the presence of Saharan dusts in this region, very few estimations of satellite  $\rho_w(\lambda)$  and in situ *chl-a* were available, and some satellite estimations of *chl-a* could present strong over-estimations (Gregg *et al*, 2004). For this reason, we reprocessed the  $\rho_w(\lambda)$  and *chl-a* data with an atmospheric correction algorithm developed specifically for Saharan dust (Diouf *et al*, 2013, <http://poac.locean-ipsl.upmc.fr>) in order to improve the satellite observations.

### 2.3 The UPSEN database

Recently, some HPLC measurements were made in the Senegalo-Mauritanian region during two oceanographic cruises (UPSEN campaigns) of the oceanographic ship “Le Suroit” from 7 to 17 March 2012 and from 5 to 26 February 2013 as reported in *Ndoye et al*, (2014); *Capet et al*, (2017). The goal was to study the dynamics and the biological variability of the Senegalo-Mauritanian upwelling. During these campaigns, in-situ HPLC measurements were carried out. We expected to be able to co-locate them with the ocean-color VIIRS (Visible Infra-red Imaging Radiometer Suite) sensor observations whose wavelengths are close to those of the SeaWiFS. Unfortunately, we were only able to process satellite observations made on 21 February 2013 due to the presence of clouds and Saharan aerosols the other days. We processed the satellite observations provided by the VIIRS sensor at four wavelengths (443, 490, 510, 555 nm) for pixels in the vicinity of the ship stations (within a distance of 20km) and observed in a time window of  $\pm 12$ h, and for which the satellite *chl-a* was less than  $3 \text{ mg m}^{-3}$ , which is the limit of validity of our method imposed by the range of *chl-a* observed in DGIP (mean of  $0.52 \text{ mg m}^{-3}$ ). Only five stations off Cabo Verde peninsula fitted these requirements (see Figure 1 for their positions).

## 3 - THE PROPOSED METHOD (2S-SOM)

Classification methods were applied for retrieving geophysical parameters from large databases in several studies including weather forecasting (*Lorenz*, 1969; *Kruizinga and Murphy*, 1983), short-term climate prediction (*Van den Dool*, 1994), downscaling (*Zorita and von Storch*, 1999), reconstruction of oceanic  $\text{pCO}_2$  (*Friedrichs and Oschlies*, 2009), and of *chl-a* concentration under clouds (*Jouini et al*, 2013). In the present study, we used a new neural network classifier, which is an extension of the SOM algorithms.

### 3-1 The SOM clustering

The SOM algorithms (*Kohonen*, 2001) constitute powerful nonlinear unsupervised classification methods. They are unsupervised neural classifiers, which have been commonly used to solve environmental problems (*Cavazos*, 1999; *Hewitson et al*, 2002; *Richardson et al*, 2003; *Liu et al*, 2005, 2006; *Niang et al*, 2003, 2006; *Reusch et al*, 2007). The SOM aims at clustering vectors  $\mathbf{z}_i \in \mathbb{R}^N$  of a multidimensional database  $\mathbf{D}$ . Clusters are represented by a fixed network of neurons (the SOM map), each neuron  $c$  being associated with the so-called referent vector  $\mathbf{w}_c \in \mathbb{R}^N$  representing a cluster. The self-organizing maps are defined as an undirected graph, usually a rectangular grid of size  $p \times q$ . This

graph structure is used to define a discrete distance (denoted by  $\delta$ ) between two neurons of the  $p \times q$  rectangular grid which presents the shortest path between two neurons. Each vector  $\mathbf{z}_i$  of  $\mathbf{D}$  is assigned to the neuron whose referent  $\mathbf{w}_c$  is the closest, in the sense of the Euclidean distance:  $\mathbf{w}_c$  is called the projection of the vector  $\mathbf{z}_i$  on the map. A fundamental property of a SOM is the topological ordering provided at the end of the clustering phase: close neurons on the map represent data that are close in the data space. The estimation of the referent vectors  $\mathbf{w}_c$  of a SOM and the topological order is achieved through a minimization process in which the referent vectors  $\mathbf{w}$  are estimated from a learning data set (The DFIG data base in the present case). The cost function is shown in Annex:

The SOMs have frequently been used in the context of completing missing data (*Jouini et al, 2013*), so the projected vectors  $\mathbf{z}_i$  may have missing components. Under these conditions, the distance between a vector  $\mathbf{z}_i \in \mathbf{D}$  and the referent vectors  $\mathbf{w}_c$  of the map is the Euclidean distance that considers only the existing components (the Truncated Distance or *TD* hereinafter).

### 3-2 The 2S-SOM Classifier

In the present case, we used the 2S-SOM algorithm, which is a modified version of the SOM, very powerful in the case of a large number of variables. It automatically structures the variables having some common characters into conceptually meaningful and homogeneous blocks. The 2S-SOM takes advantage of this structuration of  $\mathbf{D}$  and the variables into different blocks, which permits an automatic weighting of the influence of each block and consequently of each variable. The block weighting facilitates the clustering procedure by considering the most pertinent variables. The vectors of DFIG defined in section 2 can be decomposed in four blocks. The essence of this decomposition in blocks is that each of the 17 components of the DFIG vectors gathered information with a different physical influence in the classification phase. The composition of each block is done as follows:

**First Block** (B1) comprises the five pigment in-situ concentration ratios (divinyl chlorophyll-a, peridinin, fucoxanthin, 19'hexanoyloxyfucoxanthin, zeaxanthin concentration ratios). The pigment ratios are defined in Eq. 3.

**Second Block** (B2) comprises the water-leaving reflectance  $\rho_w(\lambda)$  at the five SeaWiFS wavelengths

**Third Block** (B3) comprises the five  $Ra(\lambda)$ ,

**Fourth Block** (B4) comprises two variables: The in situ and the SeaWiFS *chl-a* concentrations.

The 2S-SOM is able to deal with a large quantity of variables, choosing those that are the most significant for the classification and neutralizing those which are the least significant. This is done by

estimating weights on the blocks and the variables. We fully describe the 2S-SOM algorithm in Annex.

In the following we use a simplified version of 2S-SOM in which only the blocks are weighted.

### 3.3 The calibration phase

Similarly to the standard SOM, the 2S-SOM is determined through a learning phase by using a more complex cost function (see Annex) that estimate for each neuron, in addition to the referent vector, a weight ( $\alpha$ ) for each block. For a neuron  $c$ , we define the weights  $\alpha_{cb}$  of each block  $b$  ( $b = 1 \dots 4$ ).

At the end of the calibration phase, each element  $z_i$  of the dataset DPIG is associated with a referent  $w_c$  whose components are partitioned into four blocks. In the present study, the 2S-SOM map is represented by a two-dimensional ( $9 \times 18 = 162$ ) grid that represents the partition of the DPIG dataset into different classes. Each class provided by the 2S-SOM is associated with a so-called referent vector  $w_c$  with  $c \in \{1 \dots 162\}$ . The size of the map has been determined by using the procedure provided by the SOM software available at : <http://www.cis.hut.fi/projects/somtoolbox/download/>.

### 3.4 The Pigment retrieval

In the second phase, which is an operating phase, we estimated the pigment concentration ratios of a pixel  $PX_m$  from its satellite ocean-color sensor observations only. The 11 ocean color satellite observations ( $5 \rho_w(\lambda)$ ,  $5 Ra(\lambda)$ , and  $chl-a$ ) of pixel  $PX_m$  were projected onto the 2S-SOM using the Truncated Euclidian Distance (section 3.1). We select the neuron  $c$  associated with a referent vector whose the 11 ocean-color parameters are the closest to those observed by the satellite sensor. The pigment ratios of  $PX_m$  are those associated with the neuron  $c$ . At the end of the assignment phase, each pixel  $PX_m$  of a satellite image is associated with a referent vector  $w_c$ , which has 6 pigment concentration ratios among its 17 components. The flowcharts of the method (2S-SOM learning and pigment retrieval) are presented in Figure 4.

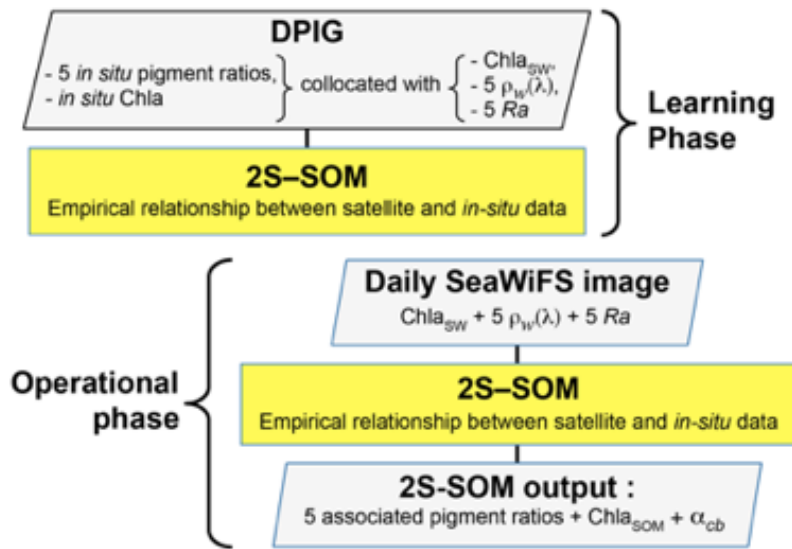


Figure 4: Flowchart of the method: top panel - Learning phase; bottom panel – operational phase which consists in pigment retrieval and the determination of the  $\alpha_{cb}$  block parameters.

## 4 - METHODOLOGICAL RESULTS

### 4-1 Statistical validation of the method

The validation of the method was focused on the retrieval of the fucoxanthin ratio, which is a characteristic of diatoms, but the same procedure could be applied to any pigment. The hyperparameter  $\mu$  (see Annex) was optimized in order to retrieve that ratio, while  $\eta$  was set constant since only the block were weighted in the present study. Due to the small amount of data in the DPIG, we estimated the accuracy of the fucoxanthin retrieval by a cross-validation procedure, which is a powerful procedure in statistics. The principle is the following: we learned 30 2S-SOM using 30 different learning datasets  $L_i$  constituted of 90% of DPIG taken at random, and then computed statistical estimator on the retrieved quantities using 30 test datasets (10% of DPIG). The algorithm was as follows:

$i=1 \dots 30$

1. determination at random of a learning dataset  $L_i$  (90% of DPIG) and a test dataset  $TL_i$  (10% of DPIG)
2. training of a 2S-SOM map  $M_i$  using  $L_i$  (see section 3.2 and 3.3).
3. Validation using  $TL_i$  according to the procedure described in section 3.4
4. Estimation of the  $RMSE_i$  and  $R^2_i$  on  $TL_i$  between the estimated and observed fucoxanthin ratios

end

Computation of the mean RMSE and  $R^2$  ( $R^2, RMSE = \frac{1}{30} \sum_{i=1}^{30} R^2_i, RMSE_i$ )

The flowchart of the cross-validation procedure is presented in Figure 5.

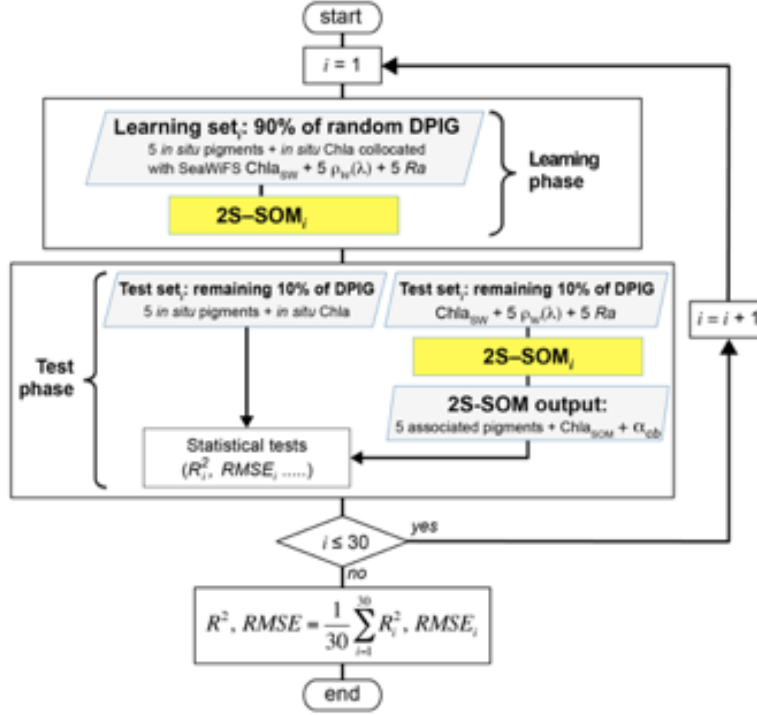


Figure 5: Flowchart of the cross-validation procedure for 30 partitions of the DPIG database.

Statistical parameters ( $R^2$  coefficients, RMSE and P-values) of the cross validation between the DPIG in situ pigments and the pigments given by the 2S-SOM averaged for the 30 2S-SOM realizations, which are presented in table 2, show the good performance of the method.

	$R^2$	RMSE [MG M <sup>-3</sup> ]	PVAL
CHLA SOM	0.84	0.22	0.001
DVCHLA	0.60	0.02	0.001
FUCO	0.87	0.02	0.001
PERID	0.81	0.01	0.001

Table 2: Statistical parameters ( $R^2$  coefficients, RMSE and P-values) of the cross validation between the DPIG in situ pigments and the pigments given by the 2S-SOM averaged for the 30 2S-SOM realizations



#### 4-2 Analysis of the topology of the 2S-SOM

As explained in sections 3-2 and 3-3, the referent vector components ( $w_c \in R^{17}$ ), which are estimated during the learning phase, are partitioned in four blocks B1, B2, B3 and B4. The hyper parameters  $\mu$  was tuned in order to favor the accuracy of the retrieval of the fucoxanthin ratio. We recall that all the pigment ratios are estimated during the calibration phase, but in the present paper attention was focused on the fucoxanthin ratio when selecting the parameter  $\mu$ . In Figure 6, we

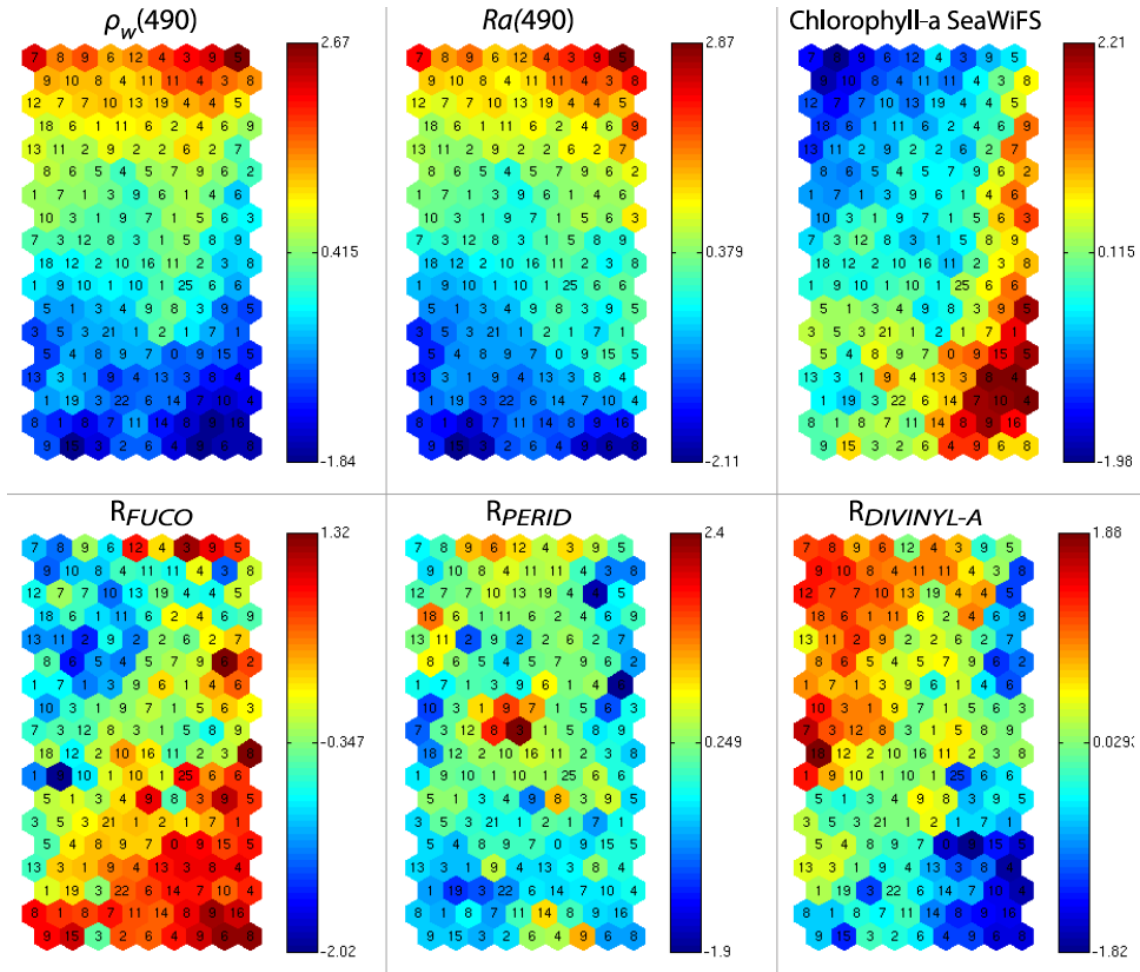


Figure 6: 2S-SOM Map. From left to right and top to bottom, values of the referent vectors for  $\rho_w(490)$ ,  $Ra(490)$ , SeaWiFS chl-a, and fucoxanthin, peridinin, divinyl Ratios. The number in each neuron indicates the amount of DPIG data captured at the end of the learning phase, the values indicated by the color bars are centered-reduced and non-dimensional values.

present six of the referent vector components of the 2S-SOM map. These components are  $\rho_w(490)$ ,  $Ra(490)$ , SeaWiFS chl-a, and the ratios of fucoxanthin, which is a specific diatom pigment, and of

*peridinin* and *divinyl*. They exhibit a coherent topological order, the components having close values being close together on the topological map. The remaining eleven components (not shown) exhibit the same coherent topological order. One can observe a very good topological order for the fucoxanthin ratio that was favored by the determination of the hyperparameter  $\mu$ . Moreover, the bottom right region in the 2S-SOM map (Figure 6) may correspond to the diatoms with a good confidence since high fucoxanthin is associated with high chlorophyll concentration and low peridinin. This is endorsed in section 5 by looking at the geographical location of the different pigment concentrations (figures 8, 10, 11). Another important remark is that the value of each component presents a large range of variation

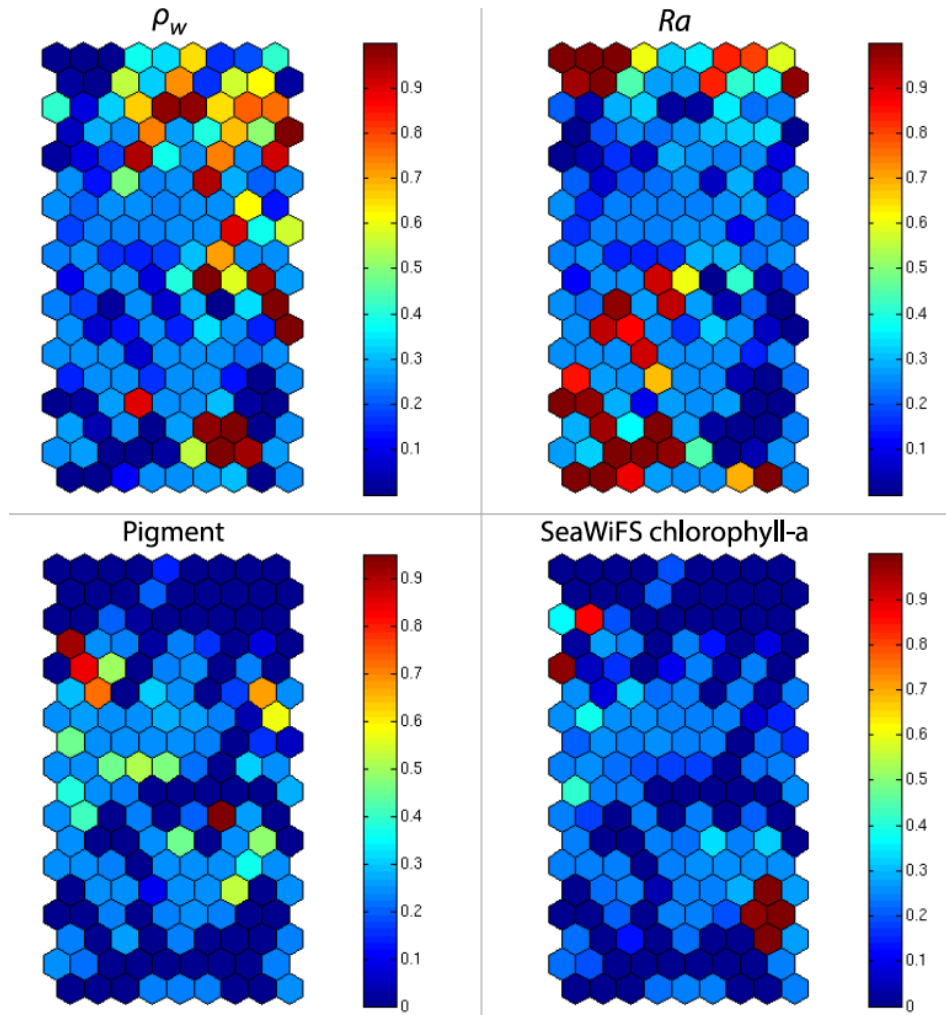


Figure 7: 2S-SOM map. Weights ( $\alpha_{cb}$ ) of the four block parameters determined at the end of the learning phase; from left to right and top to bottom:  $\rho_w$ ,  $Ra$ , Pigment, SeaWiFS chl-a. The color bars show the % of the weight estimated by 2S-SOM, a value of 1 or 0 indicating that the data in the neuron are assembled with respect to that block only.

of the same order as the range of variation found in the DFIG variables. It means that the 2S-SOM map has captured most of the variability of the dataset.

Figure 6 shows a strong link between the values of the referent vectors for fucoxanthin and *chl-a* (high fucoxanthin and *chl-a* values, at the bottom right of the 2S-SOM) while fucoxanthin is high and *chl-a* low for the referent vectors at the bottom left of the 2S-SOM. Additional information will be provided by the *Ra(490)* values when the fucoxanthin is less closely linked to the chlorophyll.

Besides, for each neuron, the 2S-SOM provides a weight for each block ( $\alpha_{cb}$ ) and each variable ( $\beta_{cbj}$ ). For a given neuron  $c$  the weights ( $\alpha_{cb}$ ) of the blocks are normalized, their sum being 1. A value of 1 for one block (and therefore a value of 0 for the other blocks) indicates that the data in the neuron are gathered with respect to that block only because there is too much noise in the variables in the other blocks. By examining the weights on the map, one can see which block most influences the link between the satellite measurements and the pigment ratios.

In Figure 7, we present the  $\alpha_{cb}$  values estimated during the learning phase of the 4 blocks (B1, B2, B3, B4). For some neurons, only the blocks related to the reflectance and the reflectance ratio are used for the definition of the neuron, while the weights for the two other blocks (pigments and *chl-a*) are null, indicating that for these neurons, in situ observations and SeaWiFS *chl-a* are more noisy than the reflectance. These neurons correspond to very small *chl-a* concentrations, which are estimated with large error. Besides, we remark that high  $\alpha$  values for *chl-a* corresponds to high *chl-a* concentration values (bottom right of the *chl-a* panel in figure 7 and figure 6 respectively). For these cases, the clustering assembled data that mainly depend on *chl-a* concentration.

## 5 - GEOPHYSICAL RESULT

In the present study, we apply the 2S-SOM (section 3), which explicitly makes a weighted use of the data according to their specificity (ocean-color signals or in situ observations) to retrieve the fucoxanthin concentration from remote sensed data in the Senegalo-Mauritanian upwelling region where in situ measurements are lacking. According to the good results of the cross-validation method as shown in section 4.1, we expect that the 2S-SOM will provide pertinent results in a region which has been poorly surveyed.

### 5-1 The pigment estimation from SeaWiFS observations in the S n galo-Mauritanian upwelling region

We decoded the DSAT database (section 2-3) using the 2S-SOM for 11 years (1998-2009) of SeaWiFS data observed in the Senegalo-Mauritanian upwelling region ( $8^{\circ}\text{N}$ - $24^{\circ}\text{N}$ ,  $14^{\circ}\text{W}$ - $20^{\circ}\text{W}$ ). This study was done according to the retrieval phase described in section 3.4. For each day, we projected the 11 SeaWiFS observations ( $5 \rho_w(\lambda)$ ,  $5 Ra(\lambda)$  and  $chl-a$ ) of each pixel  $PX_m$  on the 2S-SOM. At the end of the assignment phase, each pixel of a satellite image was associated with 6 pigment concentration ratios. The underlying assumption is that the link between the remote sensing information and the pigment ratios of a pixel is this provided by the selected referent  $w_c$ . Thanks to the topological order provided by the 2S-SOM, we expect that the best neurons chosen during the retrieval would give accurate concentration ratios. In Figures 8, 10 and 11 we present the fucoxanthin concentration ratio restitution for three different days and the associated SeaWiFS Chlorophyll images (1 and 6 January, and 28 February 2003). Due to the limited size of the DFIG, the range of the ratio learned for the

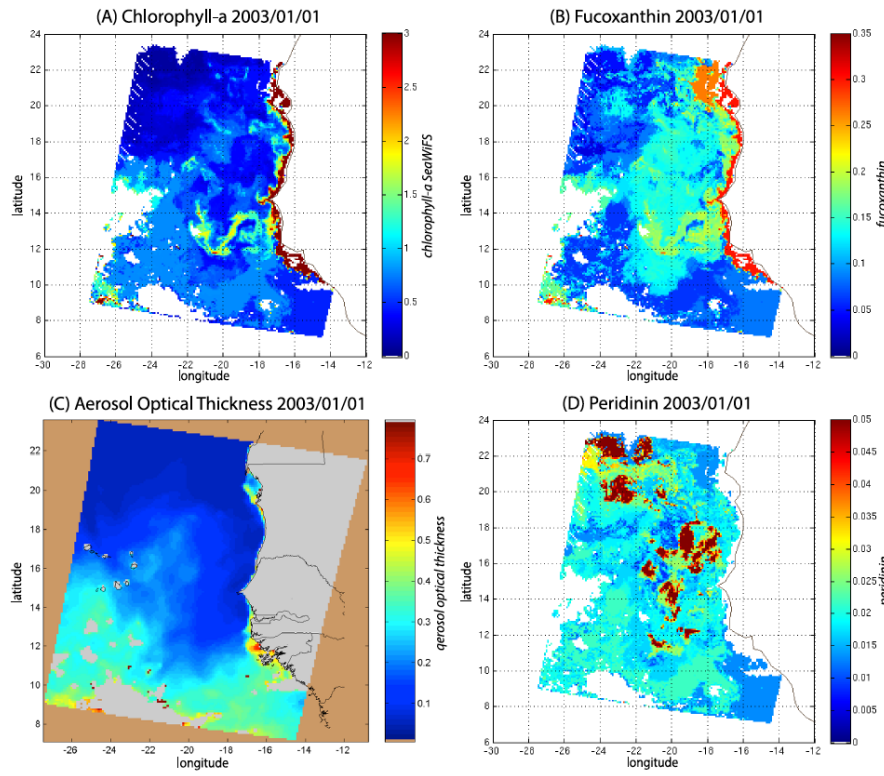
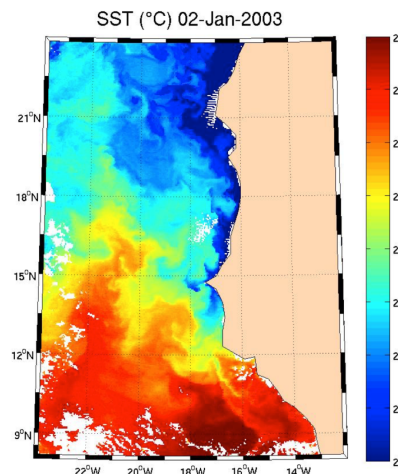
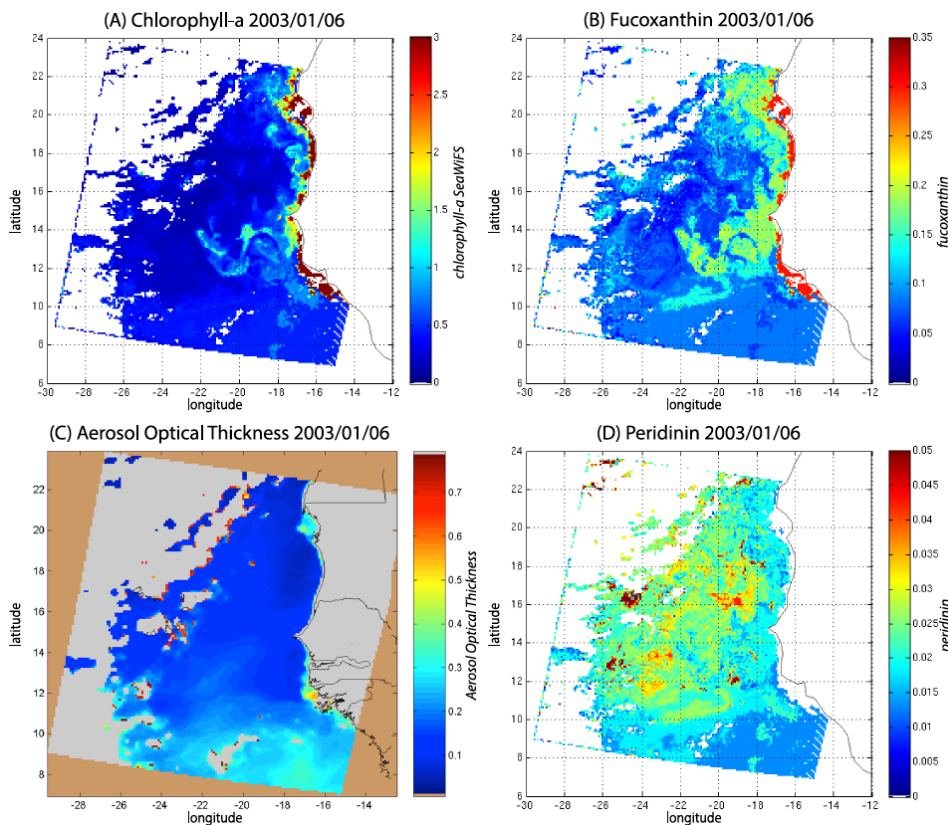


Figure 8: (A)  $chl-a$  concentration, (B) fucoxanthin ratio, (C) aerosol optical thickness, (D) peridinin for 1 January 2003. Panels (B) and (D) show that a second-order information was retrieved, which is correlated with the  $chl-a$  concentration (A) but not equivalent. The aerosol optical thickness (C) does not seem to contaminate the estimated parameters (fucoxanthin and peridinin ratios).

418 the fucoxanthin is between 0.3% and 20% with a mean of 10% and the *chl-a* content is between 0.5  
 419  $\text{mg m}^{-3}$  and  $3 \text{ mg m}^{-3}$ . The statistical estimator we used cannot extrapolate what has not been learned,  
 420



421  
 422 Figure 9: SST for 2 January 2003. Note the well-marked upwelling (cold temperature) north of 13°N.  
 423



425  
 426 Figure 10: (A) *chl-a* concentration, (B) fucoxanthin ratio, (C) aerosol optical thickness, (D) peridinin for 6  
 427 January 2003. Panels (B) and (D) show that a second-order information was retrieved, which is correlated  
 428 with the *chl-a* concentration (A) but is not equivalent. It is found that the aerosol optical thickness (C) does  
 429 not contaminate the estimated parameters (fucoxanthin and peridinin ratios).



and for that reason we flagged the pixels in the SeaWiFS images that have a *chl-a* concentration greater than 3.  $\text{mg m}^{-3}$ .

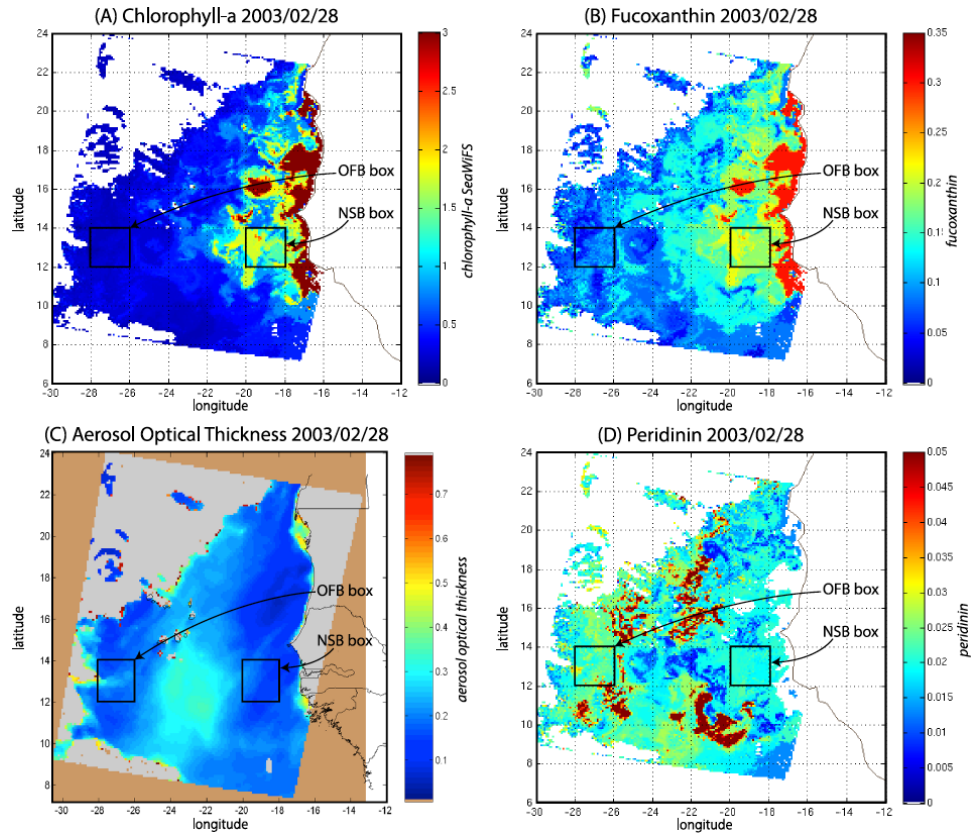


Figure 11: (A) *chl-a* concentration, (B) fucoxanthin ratio, (C) aerosol optical thickness, (D) Peridinin for 28 February 2003. Panels (B) and (D) show that a second order information was retrieved, which is correlated with the *chl-a* concentration (A) but is not equivalent. It is found that the aerosol optical thickness (C) does not contaminate the estimated parameters (fucoxanthin and peridinin ratios). The position of the NSB and OFB boxes are figured out by black square boxes

Regarding the images obtained for 1 January 2003 in the Senegalo-Mauritanian region (Fig 8A, B, C, D), we observe that the *chl-a* (Fig 8A) is very high at the coast and decreases offshore in accordance with the upwelling intensity as shown in the SST image (Fig 9). Moreover, we observed a persistent well-marked *chl-a* pattern south of the Cap Vert peninsula in form of a “W”, which is the signature of a baroclinic Rossby wave (Sirven *et al*, 2019).

Except in the southern part of the region, the AOT (Aerosol Optical Thickness) is low, which means that the atmospheric correction of the reflectance is quite small, which gives confidence in the ocean-color data products. The fucoxanthin concentration is maximum at the coast and decreases offshore as does the *chl-a* concentration, in agreement with the works of Uitz *et al.*, (2006, 2010). Fucoxanthin presents coherent spatial patterns. Peridinin concentration is somewhat complementary to that of

fucoxanthin, with the low fucoxanthin concentration area corresponding to high peridinin concentration area (northern part of Figs 8B, D). This behavior is also observed in Figure 10 (6 January 2003) and in Figure 11 (28 February, 2003) endorsing the analysis shown in Figure 8.

For 28 February, we selected two square box regions (Fig. 11), one near the coast (NSB, long  $[-20^\circ, -18^\circ]$ , lat  $[12^\circ, 14^\circ]$ ) and the other about 800 km offshore (OFB, long  $[-28^\circ, -26^\circ]$ , lat  $[12^\circ, 14^\circ]$ ). NSB waters correspond to upwelling waters while OFB waters correspond to oligotrophic waters. We projected the eleven ocean color parameters of the NSB and OFB pixels on the 2S-SOM map.

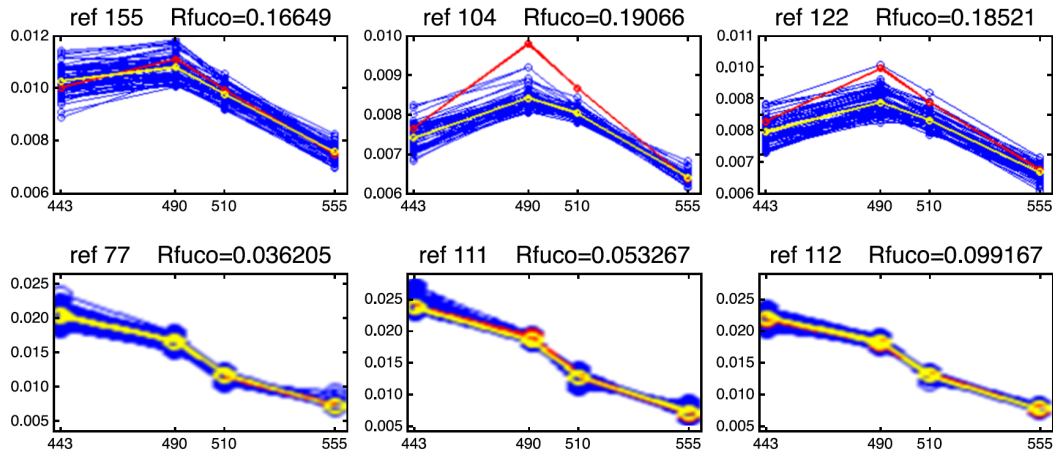


Figure 12: Reflectance spectra (in blue) captured the 28 February by six neurons whose referent vector spectra are in yellow: top line, for pixels in the NSB region (long.  $[-20^\circ, -18^\circ]$ , lat.  $[12^\circ, 14^\circ]$ ); bottom line, for pixels in the OFB region (long.  $[-28^\circ, -26^\circ]$ , lat.  $[12^\circ, 14^\circ]$ ).

Figure 12 presents the reflectance spectra (in blue) captured by three neurons of the 2S-SOM corresponding to pixels located in the NSB region (*top line*) and those captured by three neurons corresponding to pixels located in the OFB region (*bottom line*). The reflectance spectra of the associated referent vectors  $w$  are in yellow. The satellite reflectance spectra match the referent vector spectra; moreover the fucoxanthin ratio varies inversely with the mean value of the spectrum: the higher the fucoxanthin ratio, the smaller the mean value of the spectrum. The pigment concentration is greater near the coast.

We note a strong difference between the shape and the intensity of the near-shore (NSB) and offshore (OFB) spectra. The OFB spectra present mean values higher than those of the NSB spectra. This is due to the fact that NSB spectra were observed in a region where diatoms are abundant, as shown by



the high value of fucoxanthin concentration in this region (Figs 8, 10, and 11), which is a proxy for diatoms along with higher *chl-a* concentration. In Figure 12, we note the lower values of the coastal spectra at 443 nm, which can be interpreted as a predominant effect of spectral absorption by phytoplankton pigments and CDOM. The different spectra are close together in the OFB region and more disperse in the NSB region. This can be explained by the fact that the OFB region corresponds to Case-1 waters while the NSB region waters are close to Case-2 waters and are influenced by the variability of near shore process like turbidity or presence of dissolved matters, and dynamical instabilities.

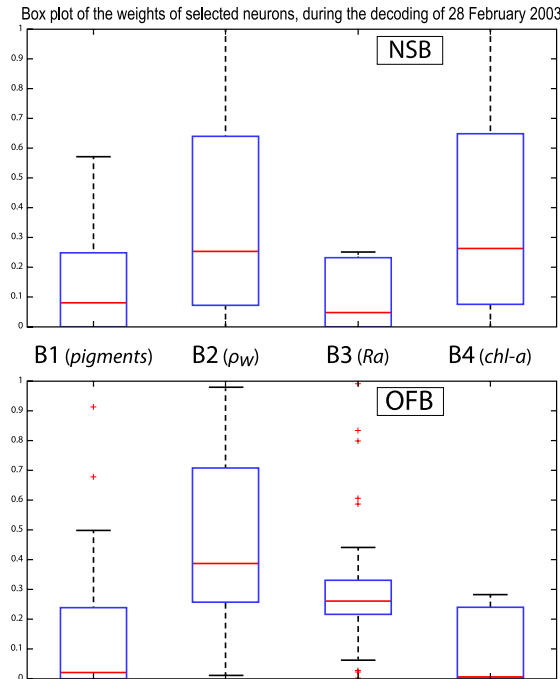


Figure 13: Box plot of the weights of the selected neurons during the decoding of the 28 February data. From left to right, weights of blocks B1, B2, B3, B4. Top panel, in the NSB region (long.  $[-20^\circ, -18^\circ]$ , lat.  $[12^\circ, 14^\circ]$ ); bottom panel, in the OFB region (long.  $[-28^\circ, -26^\circ]$ , lat.  $[12^\circ, 14^\circ]$ ).

We analyzed the weights of the blocks for the neurons selected in the analysis of the coastal (NSB) and offshore (OFB) boxes. Figure 13 presents the box plot of the weight  $\alpha_{cb}$  corresponding to the neurons belonging to the four blocks (B1, B2, B3, B4), with the constrain that the sum of the weights of a neuron is 1; a weight  $\alpha$  larger than 0.25 indicates the predominance of a block in the learning for the classification (see section 3.5). It is clear that the weights for pixels near the coast (Fig 13, top panel) are different from those for offshore pixels (Fig. 13, bottom panel). As already mentioned in section 4.3 and also shown in Figure 7, the weights of the 2S-SOM play a significant role in the 2S-SOM

topology and consequently in the pigment retrieval. The weights of blocks B1 and B4 that take into account the influence of the pigment ratios and the chlorophyll content in the retrieval are very low for the offshore (OFB) oligotrophic region and more important for the coastal (NSB) region. The weights of the blocks B2 and B3, which take into account the influence of the reflectance ( $\rho_w(\lambda)$ ,  $Ra(\lambda)$ ), dominate for the offshore regions. In coastal waters, the weights of all the blocks are used, with a smaller influence of B3, which is associated with  $R_a$ . This gives information on the role played by the different variables on the classification in waters having different phytoplankton concentration and composition. Besides it shows the automatic adaptation of the 2S-SOM to the environment in order to optimize the clustering efficiency with respect to a classical SOM.

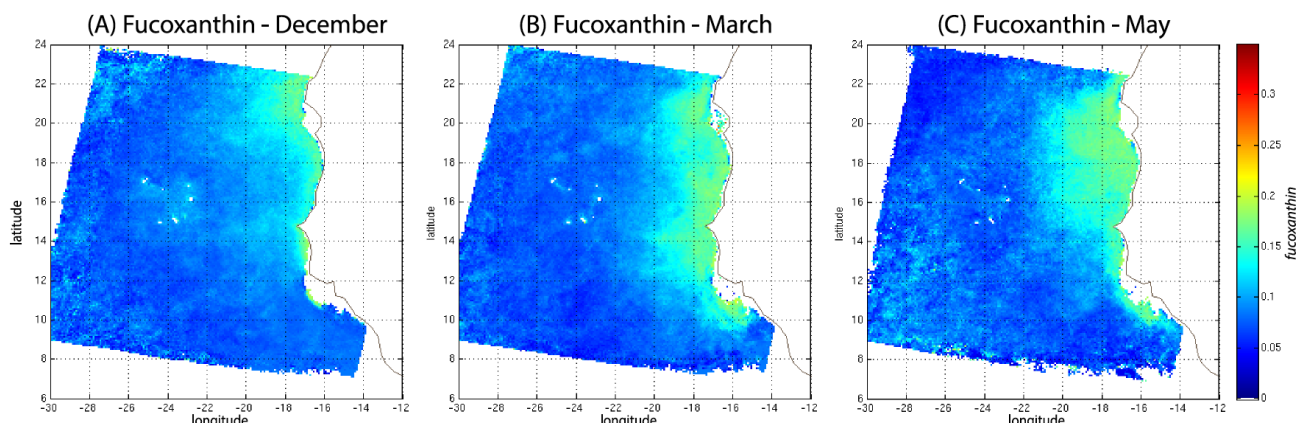


Figure 14: Monthly fucoxanthin concentration averaged for an 11- years (1998-2009) for December (A), March (B) and May (C).

In order to study the seasonal variability of the fucoxanthin concentration with some statistical confidence in the Senegalo-Mauritanian upwelling region, we constructed a monthly climatology for an 11-year period (1998–2009) of the SeaWiFS observations by summing the daily pixels of the month under study. The resulting climatology is presented in Figure 14 for December (Fig. 14a), March (Fig. 14b), and May (Fig 14c), which correspond to the most productive period (Fig. 14c). The fucoxanthin concentration, and consequently the associated diatoms, presents a well-marked seasonality. Fucoxanthin starts to develop in December North of 19°N, presents its maximum intensity in March when the upwelling intensity is maximum, extends up to the coast of Guinea (12°N) in April and begins to decrease in May where it is observed north of Cabo Verde peninsula (15°N) in agreement with the observations reported by *Farikou et al, (2015)* and *Demarcq and Faure, (2000)*.

Figure 15 shows the fucoxanthin (in green) and the *chl-a* (in blue) concentrations computed from satellite observations for an 11-year period of SeaWiFS observations in the NSB region. There is a good correlation in phase between these two variables but not in amplitude (a good coincidence of

peak occurrence but weak correlation in peak amplitude) showing that the relationship between

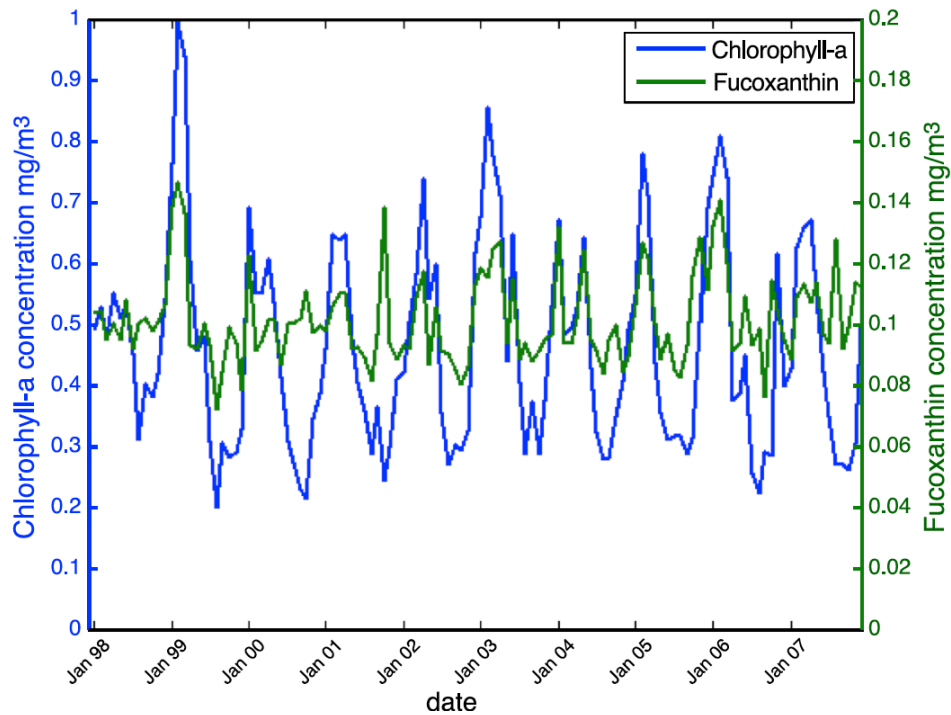


Figure 15: . *chl-a* (in blue) and *fucoxanthin* (in green) concentrations for near-shore pixels (in the NSB region).

*fucoxanthin* and *chl-a* is complex as mentioned by *Uitz et al*, (2006). In particular, there is a weak peak in *fucoxanthin* in October 2001, which is not correlated with a *chl-a* peak.

## 5-2 Analysis of the UPSEN campaigns

Figure 16 shows, for every UPSEN stations 1, 2, 3, 5a and 5b (see figure 1 for their geographical position), the averaged in-situ UPSEN spectrum (in blue), the referent spectrum (in red) of the 2S-SOM neuron captured by the collocated satellite VIIRS sensor observations. The referent spectrum is the mean of the different spectra captured by that neuron during the learning phase. Among these different spectra, there is one (black curve in figure 16) which is the closest to the UPSEN spectrum. Obviously, the black curve is closer to the blue curve than the red one which is flatten due to the averaging process. These three spectra are close together showing the good functioning of the 2S-SOM.

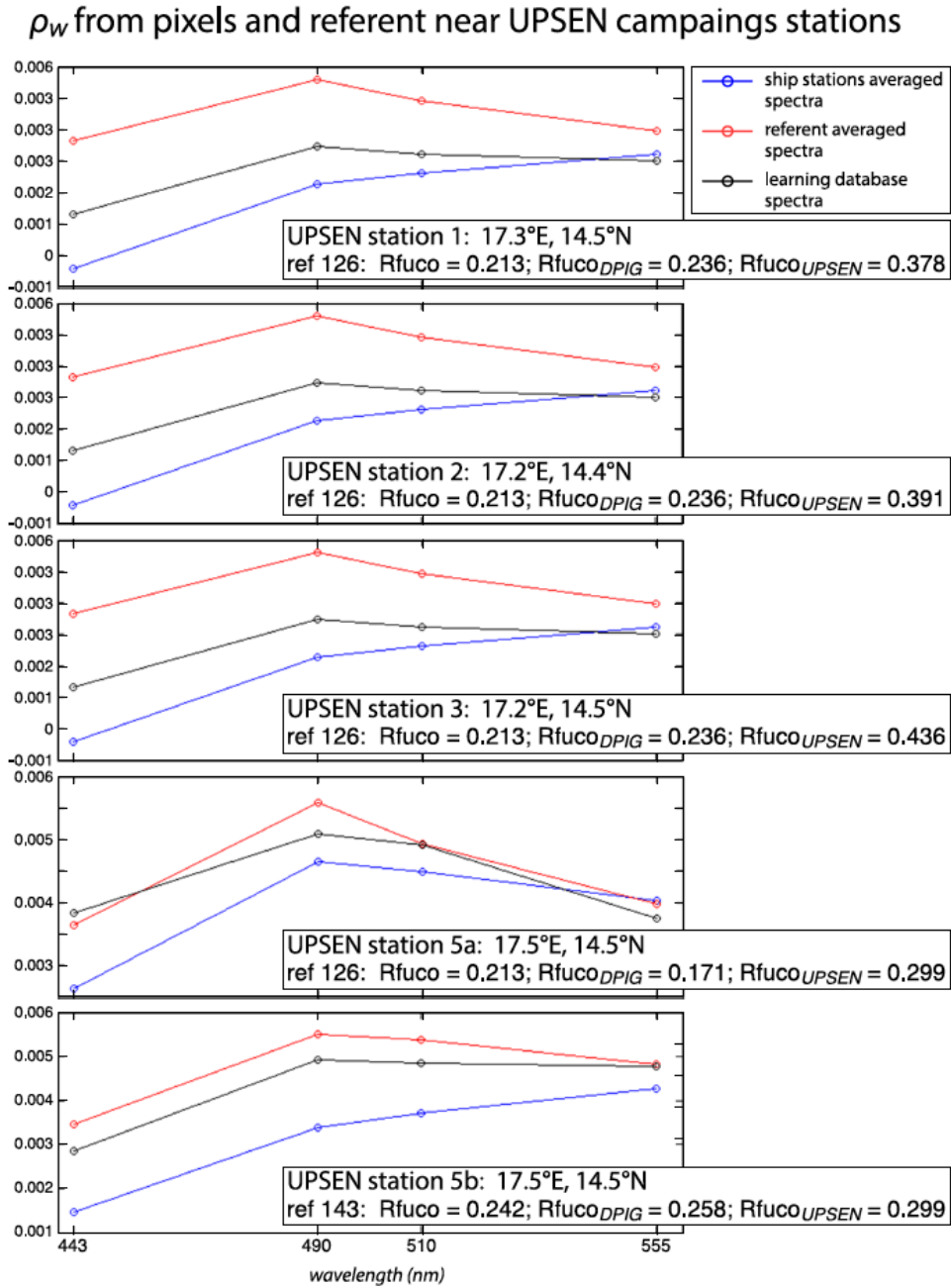


Figure 16: For ship stations 1, 2, 3, 5a and 5b, we show the averaged spectrum of the in situ spectra of the UPSEN station in blue; the spectrum of the referent vector (in red) of the 2S-SOM neuron, which has captured the closest satellite observations to the UPSEN station; among the different spectra constituting the referent spectrum, the spectrum of the learning database (DGIP) that is the closest to the averaged satellite spectra is shown in black. In the rectangular cartoons, we show the position of the UPSEN station, the number of the neuron of the 2S-SOM which has captured the satellite observation, the Rfuc of the referent vector, the Rfuc<sub>DGIP</sub> of the closest DGIP and the in situ Rfuc<sub>UPSEN</sub>.

Their shapes are close to these observed in the NSB region (Figure 12) but their intensity is lower meaning that their waters are more absorbing than the NSB waters due to a higher pigment concentration. In fact, the UPSEN stations were located close to the coast (figure 1) in the Hann bight south off the Cap Verde peninsula, which is very rich in phytoplankton pigments. In table 3, we present the fucoxanthin ratios associated with the referent vectors ( $R_{fuco2S-SOM}$ ), the closest DPIG fucoxanthin-ratios captured by the neuron of the referents and the fucoxanthin-ratios measured during the UPSEN campaign. We note that the fucoxanthin ratios of the in-situ measurements are in the range of the DPIG (see table 1), which allows a good functioning of the 2S-SOM estimator. The pigment ratios obtained from ocean-color observations through the 2S-SOM are close to pigment concentrations measured at the ship stations, which confirms the validity of the method we have developed. We remark that the best 2S-SOM estimate of fucoxanthin ratio with respect to the UPSEN in-situ measurement is given at station 5b which is the farthest off the coast. These results endorse the climatological study of the Senegalo-Mauritanian upwelling region we have done with the 2S-SOM (section 5.1).

UPSEN STATION	REFERENT N°	$R_{FUOCO}$ 2S-SOM	$R_{FUOCO}$ DPIG	$R_{FUOCO}$ UPSEN
STAT 1 17.3 E 14.5 N	126	0.213	0.236	0.378
STAT 2 17.2 E 14.4 N	126	0.213	0.236	0.391
STAT 3 17.2 E 14.5 N	126	0.213	0.236	0.436
STAT 5A 17.5 E 14.5 N	126	0.213	0.171	0.299
STAT 5B 17.5 E 14.5 N	143	0.242	0.258	0.295

Table 3: For ship stations 1, 2, 3, 5a and 5b of the UPSEN campaigns, we show the referent captured by the VIIRS observations, the fucoxanthin-ratio associated with this referent ( $R_{fuco-2S-SOM}$ ), the fucoxanthin-ratio of the closest DPIG fucoxanthin-ratio captured by the neuron of the referent and the fucoxanthin-ratio measured in situ during the UPSEN campaign

The 2S-SOM method gives pigment concentrations that are close to those obtained by in situ observations. The method could be applied to a large variety of other parameters in the context of studying and managing the planet Earth. The major constraint to obtaining accurate results is to deal with a learning data set that statistically reflects all the situations encountered in the observations processed. Due to its construction, the method cannot be used to find values beyond the range of the learning data set.

## 6 - DISCUSSION

Machine learning methods are powerful methods to invert satellite signals as soon as we have adequate database to support the calibration. Several technics have been used for retrieving biological information from ocean color satellite observations. First, studies employed multilayer perceptrons (MLP), which are a class of neural networks suitable to model transfer function (Thiria et al, 1993). Gross et al, (2000, 2004) retrieved *chl-a* concentration from SeaWiFS, Bricaud et al, (2006) modeled the absorption spectrum with MLP, Raitsos et al, 2008 and Palacz et al, 2013 introduced additional environmental variables in their MLPs such as SST in the retrieval of PSC/PFT from SeaWiFS, which improved the skill of the inversion. Another suitable procedure was to embed NN in a variational inversion, which is a very efficient way when a direct model exists (Jamet et al, 2005; Brajard et al, 2006a,b; Badran et al, 2008). Statistical analysis of absorption spectra of phytoplankton and of pigment concentrations were conducted by Chazottes et al, (2006, 2007), by using a SOM.

In the present study, due to the fact that the learning dataset was quite small (515 elements), we used an unsupervised neural network classification method, which is an extension of the SOM method well adapted to dealing with a small database whose elements are very inhomogeneous. We clustered available satellite ocean-color reflectance at five wavelengths and their derived products, such as chlorophyll concentration, and the associated in situ pigment ratios.

The major points of this study are as follows:

- The clustering was carried out by developing a new neural classifier, the so-called 2S-SOM, which presents several advantages with respect to the classical SOM. As in the SOM, we defined clusters that assemble vectors, which are close together in terms of a specified distance. This classifier was learned from a worldwide database (DPIG) whose vectors are ocean-color parameters observed by satellite multi-spectral sensors and associated pigment concentrations measured in situ. In the operational phase, SeaWiFS images are decoded, allowing the estimation of the pigment concentration ratios. The major advantage of 2S-SOM with respect to the classical SOM is to cluster variables having similar physical significance in blocks having specific weights. The weights attributed to the four blocks are computed during the learning phase and vary with the quality of the variables and with respect to their location on the ocean (near the coast or offshore). This permits to modulate the variable influence in the cost function, which makes the clustering more informative than that provided by the SOM. The block decomposition provides useful scientific information. For offshore, the weight analysis allowed us to show that more influence is given to the reflectance ratios  $Ra(\lambda)$  and less to the *chl-a* and pigment concentrations; on the contrary near the coast the weights



indicate a more active use of the pigment composition and the *chl-a* concentration. Therefore, the resulting 2S-SOM clustering therefore at best takes into account the information that belongs to the specific water content.

- The 2S-SOM decomposes the DFIG into a large number of significant ocean-color classes allowing reproduction of the different possible situations encountered in the dataset we analyze. Besides, we assume that the relationship between the pigment concentration and the remote sensed ocean-color observations is independent on the location, which is justifiable since the relationship depends on the optical properties of ocean waters through well-defined physical laws which are region-independent. This also endorses the fact that we used a global database to retrieve pigments in a definite region. On the contrary, the different phytoplankton species vary from one region to another making the relationship between pigment ratio and phytoplankton species strongly depending on the region. This justifies the fact we focused our study on the pigment retrieval rather than on the PSC or PFT, as mentioned above. Moreover, most of the recent phytoplankton in situ identifications have been made using pigment measurements with the HPLC method (*Hirata et al, 2011*). It is therefore more natural to retrieve the pigment concentrations, which is the quantity we measured, than the associated PSC or PFT, which are estimated from the pigment observations through complex non-linear and region-dependent algorithms (*Uitz et al, 2006*). Due to the characteristics of the DFIG, the method can retrieve pigment concentration patterns over a large range ( $0.02 - 2 \text{ mg m}^{-3}$ ).

- We were able to analyze the pigment concentration in the Senegalo-Mauritanian region by processing satellite ocean color observations with the 2S-SOM. We found an important seasonal signal of fucoxanthin concentration with a maximum occurring in March. We evidenced a large offshore gradient of fucoxanthin concentrations, the near shore waters being richer than the offshore ones. We showed that the offshore region waters correspond to Case-1 waters, while the near shore waters are close to Case-2 waters and are influenced by the variability of near shore process like turbidity, or the presence of dissolved matters. The UPSEN measurements show that the pigment ratios of the Senegalo-Mauritanian region are in the range of the DFIG database used to calibrate the method, which justifies the use of the 2S-SOM algorithm to investigate this region.

- We used daily satellite observations to construct a monthly climatology of pigment concentrations of the Senegalo-Mauritanian upwelling region, which has been poorly surveyed by oceanic cruises. Due to the highly non-linear character of the algorithms for determining the pigment concentrations from satellite measurements, it is mathematically more rigorous to apply these algorithms to daily satellite data and to average this daily estimate for the climatology period under study, than to estimate them from the satellite data climatology, as many authors have done (*Uitz et al., 2010; Hirata et al., 2011*). We found that Fucoxanthin starts developing in December North of  $19^{\circ}\text{N}$ ,



presents its maximum intensity in March when the upwelling intensity is maximum, extends up to the coast of Guinea (12°N) in April and begins to decrease in May

Another important aspect of our study concerns the validity of our results. The 2S-SOM method has been validated by focusing the retrieval accuracy on the fucoxanthin ratio, by using a cross-validation procedure. These results were qualitatively confirmed by two other independent studies.

- We first applied a cross validation procedure (see section 4.1), which is powerful technique for validating models (*Kohavi, 1995; Varma and Simon, 2006*). We learned 30 different 2S-SOM using 30 different learning dataset determined at random from the DPIG dataset (each learning dataset representing 90% of DPIG) and 30 test datasets (10% of DPIG). By averaging the results, we found that the 2S-SOM method retrieves the fucoxanthin concentration with a good score (see the statistical parameters in table 2) which confirms the pertinence of the method.

- We then found that our fucoxanthin climatology is in agreement with in situ observations of phytoplankton reported in *Blasco et al. (1980)* in March to May 1974 off the coast of Senegal during the JOINT I experiment. These authors analyzed 740 water samples collected with Niskin bottles at 136 stations extending along a line at 21°40'N (in the northern part of the studied region) from 0 to 100 km offshore. The samples were taken at several depths (mostly at 100, 50, 30, 15, 5 m). Phytoplankton cells were counted and identified by the Utermohl inverted microscope technique (*Blasco, 1977*). These authors found that diatoms reach their maximum concentration in April–May and are the most abundant group in that period, whereas the other cells predominate in March. Similar microscope observations have been reported in the ocean area south of Dakar by *A. Dia (1985)* during several ship surveys in February–March 1982–1983.

- Our method is also in agreement with the monthly eleven years climatology presented in *Farikou et al, (2015)* who used a modified PHYSAT method to retrieve the *PFT* in the Senegalo-Mauritanian region.

- The pigment concentrations provided by the 2S-SOM from the VIIRS sensor observations are in qualitative agreement with the in-situ measurements done at five stations during the two UPSEN campaigns in 2012 and 2013, showing that the method is able to function in waters where the pigment concentrations are quite high (fucoxanthin ratios of the order 0.4).

## 7 - CONCLUSION

We developed a new neural network clustering method, the so-called 2S-SOM algorithm to retrieve phytoplankton pigment concentration from satellite ocean color multi spectral sensors. The 2S-SOM algorithm is a SOM specifically designed to deal with a large number of heterogeneous components such as optical and chemical measurements. The major advantage of 2S-SOM with respect to the classical SOM is to cluster variables having similar significance in blocks having specific weights. The weights attributed to the blocks during the learning phase vary with the quality of the variables in the classification. This permits to modulate the variable influence in the cost function, which makes the clustering more informative than that provided by the SOM. Besides, the block weighting provides useful information on the functioning of the classification by permitting to identify the variables which control it. It also allows us to better understand the dynamics of the phytoplankton communities.

The 2S-SOM method is efficient and rapid as soon as the calibration is done, since it uses elementary algebraic operations only. The 2S-SOM method is like a piecewise regression that takes advantage of the unsupervised classification of the SOM. We decomposed the DFIG database into quite a large number of partitions ( $9 \times 8 = 162$ ) when comparing our study to other studies (*Uitz et al*, 2006, 2012). The validity of the method has been controlled through a cross validation procedure and confirmed by three qualitative studies. Statistical parameters ( $R^2$  coefficients, RMSE and P-values) of the cross-validation between the DFIG in situ pigments and the pigments given by the 2S-SOM averaged for the 30 2S-SOM realizations presented in table 2, show the good performance of the method. It must be noticed that the performance mainly depends on the size of the learning set used to calibrate the 2S-SOM. This set must include all the situations encountered in the pigment retrieval. The larger the learning set, the better the method performs. Due to its generic character and its flexibility, the method could be used to determine a large variety of measures done with satellite remote sensing observations.

In this work, the method was applied to study the seasonal variability of the fucoxanthin concentration in Senegalo-Mauritanian upwelling region. We showed a large offshore gradient of fucoxanthin, the higher concentration being situated near the shore. We were able to construct a monthly climatology for an 11-year period (1998–2009) of the SeaWiFS observations by summing the daily pixels of the month under study in a region which was poorly surveyed by oceanic cruises. The fucoxanthin concentration, and consequently the associated diatoms, present a well-marked seasonality (Figure 10). Fucoxanthin starts developing in December North of  $19^\circ\text{N}$ , presents its maximum intensity in March when the upwelling intensity is maximum, extends up to the coast of Guinea ( $12^\circ\text{N}$ ) in April and begins to decrease in May where it is observed north of Cabo Verde peninsula ( $15^\circ\text{N}$ ), in agreement

with the observations reported by *Farikou et al*, (2015) and *Demarcq and Faure*, (2000). The UPSEN campaign results endorse the validity of the study of the Senegalo-Mauritanian upwelling region done with the 2S-SOM.

### **Acknowledgments**

The study was supported by the projects CNES-TOSCA 2013-2014 and 2014-2015. The water-leaving reflectances were obtained from the SeaWiFS daily reflectances,  $\rho_{\text{obsTOAw}}(\lambda)$ , provided by the NASA/GSFC/DAAC observed at the top of the atmosphere (TOA) and processed with the SOM-NV algorithm (Diouf et al., 2013) from 1998 to 2010. They are available at the web site: <http://poacc.locean-ipsl.upmc.fr/>. The DPIG data base was kindly provided by Dr. S. Alvain. We thank Dr. Alban Lazar and Dr. E. Machu for providing in situ data measured during the UPSEN experiments as well as stimulating discussions for their interpretation. We also thank Ray Griffiths for editing the manuscript.

## References

- Alvain S, Moulin C., Dandonneau Y. and Breon F. M. : Remote sensing of phytoplankton groups in case-1 waters from global SeaWiFS imagery. *Deep-Sea Res. Part1*, V **52** (11), pp 1989-2004, 2005.
- Alvain, S. Loisel H. and Dessailly D. : Theoretical analysis of ocean color radiances anomalies and implications for phytoplankton group detection. *Optics Express*, V **20** (2), 2012.
- Antoine D., André J. M. , Morel A. : Oceanic primary production : Estimation at global scale from satellite (Coastal Zone Color Scanner) chlorophyll. *Global Biogeochem Cy.* V **10**, pp 57-69, 1996.
- Badran F., Berrada M. , Brajard J., Crepon M. , Sorrow C., Thiria S., Hermand J.P. , Meyer M., Perichon L., Asch M. : Inversion of satellite ocean colour imagery and geoacoustic characterization of seabed properties : Variational data inversion using a semi-automatic adjoint approach *J. Marine Systems*, V **69**, pp 126-136, 2008
- Behrenfeld M. J., Boss E., Siegel D.A., Shea D.M. : Carbon-based ocean productivity and phytoplankton physiology from space. *Global Biogeochem. Cy.* V **19**, GB1006, doi:10.1029/2004GB002299, 2005
- Behrenfeld M. J., and Falkowski P.G. : Photosynthetic rates derived from satellite base chlorophyll concentration. *Limnol. Oceanogr.* V **42**, pp 1-20, 1997
- Ben Mustapha Z. S., Alvain S. , Jamet C., Loisel H. and Desailly D. : Automatic water leaving radiance anomalies from global SeaWiFS imagery: application to the detection of phytoplankton groups in open waters. *Remote Sens. Environ.*, vol 146, pp 97-112, 2014.
- Blasco D. : Red tide in the upwelling region of Baja California. *Limnol. Oceanogr.* vol 22, pp 255-263, 1977
- Blasco D., Estrada M. and Jones B. : Relationship between the phytoplankton distribution and composition and the hydrography in the northwest African upwelling region, near Cabo Corbeiro. *Deep-Sea Res.* , vol 27A, pp 799-821, 1980.
- Bracher A., Bouman HA, Brewin RJW, Bricaud A, Brotas V, Ciotti AM, Clementson L, Devred E, Di Cicco A, Dutkiewicz S, Hardman-Mountford NJ, Hickman AE, Hieronymi M, Hirata T, Losa SN, Mouw CB, Organelli E, Raitsos DE, Uitz J, Vogt M and Wolanin A : Obtaining Phytoplankton Diversity from Ocean Color: A Scientific Roadmap for Future Development. *Front. Mar. Sci.* 4:55. doi: 10.3389/fmars.2017.00055, 2017
- Brajard J., Jamet C., Moulin C. and Thiria S. : Atmospheric correction and oceanic constituents retrieval with a neuro-variational method. *Neural Networks*, Vol 19(2), p178-185, 2006

- 774 Brajard J., Jamet C., Moulin C. and Thiria S : Neurovariational inversion of ocean color images. J.  
775 Atmos. Space Res. Vol 38, n 2, pp 2169-2175, 2006
- 776 Brewin R. J. W., Hardman-Mountford N. J., Lavender S. J., Raitos D. E., Hirata T., Uitz J., et al. :  
777 An inter-comparison of bio-optical techniques for detecting dominant phytoplankton size class  
778 from satellite remote sensing. Remote Sens. Environ. 115, 325–339. doi:  
779 10.1016/j.rse.2010.09.004, 2011
- 780 Brewin R. J. W., Sathyendranath S., Hirata, T., Lavender, S.J., Barciela, R., Hardman-Montford, N.J :  
781 A three-component model of phytoplankton size class for the Atlantic Ocean. Ecol. Model. vol **22**,  
782 pp 1472-1483, 2010.
- 783 Bricaud A., Mejia C. , Blondeau Patissier D. , Claustre H., Crepon M. and Thiria S. : Retrieval of  
784 pigment concentrations and size structure of algal populations from absorption spectra using  
785 multilayered perceptrons. Applied Optics Mars 2007 vol 46 n°8., 2006
- 786 Capet X., Estrade, P., Machu, E., Ndoeye, S. et al. : On the Dynamics of the Southern Senegal  
787 Upwelling Center: Observed Variability from Synoptic to Superinertial Scales : J. Phys. Oceanogr.  
788 vol **47** (1), pp 155-180, 2017
- 789 Cavazos T. : Using Self-Organizing Maps to Investigate Extreme Climate Events: An Application to  
790 Wintertime Precipitation in the Balkans. J. Climate, vol **13**, 1718–1732, 2000.
- 791 Chazotte A., Crepon M., Bricaud A., Ras J. and Thiria S. : Statistical analysis of absorption spectra  
792 of phytoplankton and of pigment concentrations observed during three POMME cruises using a  
793 neural network clustering method. Applied Optics, 46 (18), 3790-3799, 2007
- 794 Chazottes A., Bricaud A., Crepon M. and Thiria S. : Statistical analysis of a data base of absorption  
795 spectra of phytoplankton and pigment concentrations using self-organizing maps. Appl. Opt. 45,  
796 8102-8115, 2006
- 797 Ciotti A. and Bricaud A. : Retrievals of a size parameter for phytoplankton and spectral light absorption  
798 by colored detrital matter from water-leaving radiances at SeaWiFS channels in a continental shelf  
799 region off Brazil. Limnol. Oceanogr. Methods, vol **4**, pp 237-253, 2006.
- 800 Demarcq H. and Faure V. : Coastal upwelling and associated retention indices from satellite SST.  
801 Application to Octopus vulgaris recruitment. Oceanografica Acta, vol **23**, pp 391-407, 2000.
- 802 Dia A. Biomasse et biologie du phytoplancton le long de la petite côte sénégalaise et relations avec  
803 l'hydrologie. Rapport interne N°44 du CRODT, Réf: 0C000798, 1981-1982. On line on the web  
804 site:<http://www.sist.sn/gsd/collect/publi/index/assoc/HASH2127.dir/doc.pdf>
- 805 Diouf D., Niang A., Brajard J., Crepon M. and Thiria S. : Retrieving aerosol characteristics and sea-  
806 surface chlorophyll from satellite ocean color multi-spectral sensors using a neural-variational  
807 method. Remote Sens. Environ. vol **130**, pp 74-86, 2013.

- 808 Farikou O., Sawadogo S., Niang A., Brajard J., Mejia C., Crépon M. and Thiria S. : Multivariate  
 809 analysis of the S n galo-Mauritanian area by merging satellite remote sensing ocean color and SST  
 810 observations. *J. Environ. Earth Sci.* vol **5** (12), pp 756-768, 2013
- 811 Farikou O., Sawadogo S., Niang A., Diouf D., Brajard J., Mejia C., Dandonneau Y., Gasc G., Crepon  
 812 M., and Thiria S. : Inferring the seasonal evolution of phytoplankton groups in the S n galo-  
 813 Mauritanian upwelling region from satellite ocean-color spectral measurements, *J. Geophys. Res.*  
 814 *Oceans*, vol **120**, pp 6581-6601, 2015.
- 815 Friedrich T. and Oeschies A. : Basin-scale pCO<sub>2</sub> maps estimated from ARGO float data : A model  
 816 study, *J. Geophys. Res.*, vol **114**, C10012, doi: 10. 1029/2009JC005322, 2009.
- 817 Gordon H. R. : Atmospheric correction of ocean color imagery in the Earth Observing System era. *J.*  
 818 *Geophys. Re. Atmospheres*, vol **102**(D14), pp 17081-17106, 1997.
- 819 Hewitson B.C. and Crane R. G. : Self organizing maps : application to synoptic climatology. *Climate*  
 820 *research*, vol **22**, pp 13-26, 2002
- 821 Gross L., Frouin R., Dupouy C., Andre J. M. and Thiria S. : Reducing biological variability in the  
 822 retrieval of chlorophyll\_a concentration from spectral marine reflectance. *Applied Optics*, Vol. 43  
 823 Issue 20 pp. 4041, 2004
- 824 Gross L., Thiria S., Frouin R., Mitchell B.G : Artificial neural networks for modeling transfer  
 825 function between marine reflectance and phytoplankton pigment concentration *J. Geophys. Res.*  
 826 Vol 105,no.C2, pp3483-3949, february 15, 2000.
- 827 Hirata T. , Aiken J., Hardman-Mountford N., Smyth T. J. and Barlow R.G. : An absorption model to  
 828 determine phytoplankton size classes from satellite ocean color, *Remote Sens. Environ.* vol **112**, pp  
 829 3153-3159, 2008.
- 830 Hirata T. , Hardman-Mountford N.J., Brewin R.J.W., Aiken J., Barlow R., Suzuki K., Isada T., Howell  
 831 E., Hashioka T., Noguchi-Aita M. and Yamanaka Y. : Synoptic relationships between surface  
 832 chlorophyll-*a* and diagnostic pigments specific to phytoplankton functional types. *Biogeosciences*,  
 833 vol **8** (2): pp 311-327, 2011.
- 834 Jamet C., Thiria S., Moullin C., Crepon M. : Use of a neural inversion for retrieving Oceanic and  
 835 Atmospheric constituents for Ocean Color imagery : a feasibility study.  
 836 doi:10.1175/JTECH1688.1, *J. Atmos. Ocean. Techno.* :/ Vol. 22, No. 4, pp. 460–475, 2005
- 837 Jeffreys S.W. and Veski M. : Phytoplankton Pigment in Oceanography : Guidelines to Modern  
 838 Methods, UNESCO, Paris, ed S. W. Jeffery, R.F.C. Mantoura and S. W. Wright, Introduction to  
 839 marine phytoplankton and their pigment signatures, pp 33-84, 1997.
- 840 Jouini M., L vy M. , Cr pon M. and Thiria S. : Reconstruction of ocean color images under clouds  
 841 using a neuronal classification method. *Remote Sens. Environ.* vol **131**, pp 232-246, 2013

- 842 Kohavi R. : A study of cross-validation and bootstrap for accuracy estimation and model selection.  
 843 Proceedings of the Fourteenth International Joint Conference on Artificial Intelligence. San Mateo,  
 844 CA: Morgan Kaufmann ed.. **2** (12): pp 1137–1143, 1995.
- 845 Kohonen T : Self-organizing maps (3<sup>rd</sup> ed.). Springer, Berlin Heidelberg New York. 2001
- 846 Kruizinga S. and Murphy A : Use of an analogue procedure to formulate objective probabilistic  
 847 temperature forecasts in the Netherlands. Mon. Wea. Rev., vol **111**, pp 2244–2254, 1983.
- 848 Le Quéré et al, (2018) : Global Carbon Budget 2018, *Earth Syst. Sci. Data*, **10**, 2141–2194, 2018 ;  
 849 <https://doi.org/10.5194/essd-10-2141-2018>
- 850 Lévy M., D. Iovino, L. Resplandy, P. Klein, G. Madec, A.-M. Tréguier, S. Masson, K. Takahashi, Large-scale  
 851 impacts of submesoscale dynamics on phytoplankton: Local and remote effects, *Ocean Modelling*, **77–93**,  
 852 **2012**
- 853 Levy, M., Mesoscale variability of phytoplankton and of new production: Impact of the large-scale nutrient  
 854 distribution, *J. Geophys. Res.*, **108(C11)**, 3358, doi:10.1029/2002JC001577, 2003.
- 855 Liu Y. and Weisberg R. H. : Patterns of ocean current variability on the West Florida Shelf using the  
 856 self-organizing map, *J. Geophys. Res.*, **110**, C06003, doi:10.1029/2004JC002786, 2005
- 857 Liu Y., Weisberg R. H., and He R. : Sea surface temperature patterns on the West Florida Shelf using  
 858 growing hierarchical self-organizing maps, *J. Atmos. Oceanic Technol.*, vol **23**(2), pp 325–338, 2006
- 859 Longhurst A. R., Sathyendranath S., Platt T., Caverhill C. : An estimation of global primary production  
 860 in the ocean from satellite radiometer data. *J. Plank. Res.* vol **17**, pp 1245–1271, 1995
- 861 Lorenz E. N : Atmospheric predictability as revealed by naturally occurring analogs. *J. Atmos. Sci.*,  
 862 vol 26, pp 639–646, 1969
- 863 Morel A. and Gentili G. : Diffuse reflectance of oceanic waters. III. Implication of bidirectionality for  
 864 the remote-sensing problem. *Appl. Opt.* vol 35, pp 4850–4862, 1996.
- 865 Mouw C. B. and Yoder J. A. : Optical determination of phytoplankton size composition from global  
 866 SeaWiFS imagery. *J. Geophys. Res.* vol **115**, C12018, doi:10.1029/2010JC006337, 2010.
- 867 Ndoye S. , Capet X., Estrade P., Sow B., Dagorne D., Lazar A., Gaye A. and Brehmer P. : SST patterns  
 868 and dynamics of the southern Senegal-Gambia upwelling center. *J. Geophys. Res. Oceans*, vol 119,  
 869 pp 8315–8335. 2014
- 870 Niang, A., Gross, L., Thiria, S., Badran, F., & Moulin, C. Automatic neural classification of ocean  
 871 colour reflectance spectra at the top of atmosphere with introduction of expert knowledge.  
 872 *Remote Sens. Environ.*, vol 86, pp 257–271, 2003.
- 873 Niang A., Badran F., Moulin C., Crépon M. and Thiria S. : Retrieval of aerosol type and optical  
 874 thickness over the Mediterranean from SeaWiFS images using an automatic neural classification  
 875 method. *Remote Sens. Environ.* vol 100, pp 82–94, 2006.



- 876 O'Reilly, J.E., Maritorena, S., Siegel, D. A., O'Brien, M. C., Toole, D., Mitchell, B. G., Kahru, M.,  
 877 Chavez, F. P., Strutton, P., Cota, G. F., Hooker, S. B., McClain, C. R., Carder, K. L., Muller-  
 878 Karger, F., Harding, L., Magnuson, A., Phinney, D., Moore, G.F., Aiken, J., Arrigo, K. R.,  
 879 Letelier, R., and Culver, M. Ocean color chlorophyll a algorithms for SeaWiFS, OC2 and  
 880 OC4: Version 4. In S. B. Hooker, and E. R. Firestone (Eds), *SeaWiFS postlaunch calibration and*  
 881 *validation analyses: Part 3. NASA Tech. Memo. 2000-206892, vol. 11*(pp.9-23). Greenbelt, MD:  
 882 NASA Goddard Space Flight Center. 2001.
- 883 Palacz A. P., St. John, M. A., Brewin, R. J.W., Hirata, T., and Gregg, W.W. : Distribution of  
 884 phytoplankton functional types in high-nitrate low-chlorophyll waters in a new diagnostic  
 885 ecological indicator model. *Biogeosciences* 10, 7553–7574. doi: 10.5194/bg-10-7553, 2013.
- 886 Raitsos D. E., Lavender, S. J., Maravelias, C. D., Haralambous, J., Richardson, A. J., and Reid, P.  
 887 C. : Identifying phytoplankton functional groups from space: an ecological approach. *Limnol.*  
 888 *Oceanogr.* 53, 605–613. doi: 10.4319/lo.2008.53.2.0605, 2008
- 889 Reusch D. B., Alley, R. B., and Hewitson, B. C : North Atlantic climate variability from a self-  
 890 organizing map perspective, *J. Geophys. Res.*, vol **112**, D02104, doi:10.1029/2006JD007460, 2007.
- 891 Sathyendranath S., Watts S., L., Devred E., Platt T., Caverhill C. M., and Maass H. : Discrimination  
 892 of diatom from other phytoplankton using ocean-colour data, *Mar. Ecol. Prog. Ser.*, vol 272, pp 59–  
 893 68, 2004.
- 894 Sirven J., Mignot J., Crépon M. : Generation of Rossby waves off the Cap Verde Peninsula: the role  
 895 of the coastline . *Ocean Sci.*, 15, 1–24, 2019
- 896 Sosik, H.M.; Sathyendranath, S.; Uitz, J.; Bouman, H.; Nair, A. In situ methods of measuring  
 897 phytoplankton functional types. In *Phytoplankton Functional Types from Space*. IOCCG report, No.  
 898 15; Sathyendranath, S., Ed.; IOCCG: Dartmouth, NS, Canada, pp. 21–38, 2014.
- 899 Uitz J., Claustre H., Morel A. and. Hooker S.B : Vertical distribution of phytoplankton communities  
 900 in open ocean: an assessment based on surface chlorophyll. *J. Geophys. Res.* **111**, C08005,  
 901 doi:10.1029/2005JC003207. 2006
- 902 Uitz J., Claustre H., Gentili B. and Stramski D. : Phytoplankton class-specific primary production in  
 903 the world's ocean: seasonal and interannual variability from satellite observations. *Global*  
 904 *Biogeochem. Cycles*, vol **24**, GB 3016, doi:10.1029/2009GB003680, 2010
- 905 Van den Dool H. : Searching for analogs, how long must we wait? *Tellus*, vol **46A**, pp 314–324, 1994.
- 906 Varma, S., Simon, R. : Bias in error estimation when using cross-validation for model selection; *BMC*  
 907 *Bioinformatics*. vol 7. PMC 1397873 . PMID 16504092. doi:10.1186/1471-2105-7-91, 2006



- 908 Vidussi F., Claustre H., Manca B. B., Luchetta A. and Marty J. C. : Phytoplankton pigment distribution  
909 in relation to upper thermocline circulation in the eastern Mediterranean sea during winter. J.  
910 Geophys. Res., vol 106, pp 19,939-19,956, 2001.
- 911 Westberry T., Behrenfeld M.J., Siegel D. A. and Boss E.: Carbon-based productivity modeling with  
912 vertically resolved photoacclimation. Global Biogeochem. Cycles, vol **22**, *GB2024*,  
913 DOI:10.1029/2007GB003078, 2008
- 914 Zorita E. and Von Storch H. : The Analog Method as a Simple Statistical Downscaling Technique:  
915 Comparison with More Complicated Methods. Journal of Climate, vol **12**, pp 2474-2489, 1999.
- 916

## ANNEX 1

### A1 Cost function of the SOM

Let us recall the following notation:

$\mathbf{D} = \{\mathbf{z}_1, \dots, \mathbf{z}_i, \dots, \mathbf{z}_K\}$  the dataset composed of  $K$  vectors  $\mathbf{z}_i \in \mathbb{R}^N$

$\mathbf{W} = \{\mathbf{w}_1, \dots, \mathbf{w}_c, \dots, \mathbf{w}_C\}$  the set of weights  $\mathbf{w}_c \in \mathbb{R}^N$  where  $C = p \times q$  is the size of the SOM.

The  $\mathbf{w}_c$  of the SOM are estimated by minimizing a cost function of the form

$$J_{SOM}^T(\chi, \mathbf{W}) = \sum_{i=1}^K \sum_{c=1}^{p \times q} K^T(\delta(c, \chi(\mathbf{z}_i))) \|\mathbf{z}_i - \mathbf{w}_c\|^2, \quad (A.1)$$

where  $c$  indices the neurons of the SOM map,  $\chi$  is the allocation function that assigns each element  $\mathbf{z}_i$  of  $\mathbf{D}$  to its referent vector  $\mathbf{w}_c$  which is of the form  $\chi(\mathbf{z}_i) = \arg \min_c \|\mathbf{z}_i - \mathbf{w}_c\|^2$ ,

$\delta(c, \chi(\mathbf{z}_i))$  is the discrete distance on the SOM between a neuron of index  $c$  and the neuron allocated to observation  $\mathbf{z}_i$ , and  $K^T$  a kernel function parameterized by  $T$  that weights the discrete distance on the map and decreases during the minimization process.  $T$  acts as a regularization term (Kohonen, 2001, Niang et al, 2003). In the present case  $K^T$  is of the form :

$K^T(\delta) = (1/T)K(\delta/T)$ , where  $K$  is the gaussian function of mean 0 and standard deviation 1.

The cost function (A1) takes into account the proper inertia of the partition of the data set  $\mathbf{D}$  and ensures that its topology is preserved.

### A2 Definition of the Algorithm 2S-SOM

The 2S-SOM algorithm is an extension of the Self-Organizing maps (SOM, Kohonen, 2001) based on the K-mean method (Ouattara et al., 2014, <https://www.theses.fr/179489704>). It automatically structures the variables having some common characters into conceptually meaningful and homogeneous blocks during the learning phase. The 2S-SOM takes advantage of this structuration of  $\mathbf{D}$  and the variables into  $B$  different blocks, which permits an automatic weighting of the influence of each block and consequently of each variable in the classification phase. The 2S-SOM is based on a modification of the cost function of the SOM algorithm. For a neuron of index  $c$ , we define the weights  $\alpha_{cb}$  of each block  $b$  ( $b = 1, \dots, B$ ) and the weights  $\beta_{cbj}$  of the variables  $j$  ( $j = 1, \dots, P_b$ ) in this block, where  $P_b$  is the number of variable in the block indexed by  $b$ . The vectors of weights are denoted

$$\boldsymbol{\alpha} = \{\alpha_{cb}\}_{1 \leq c \leq C, 1 \leq b \leq B} \text{ and } \boldsymbol{\beta} = \{\beta_{cbj}\}_{1 \leq c \leq C, 1 \leq b \leq B, 1 \leq j \leq P_b}$$

The new cost function is:

$$J_{2S-SOM}^T(\chi, \mathbf{W}, \boldsymbol{\alpha}, \boldsymbol{\beta}) = \sum_c \left( \sum_{b=1}^B \left( \sum_{zi \in D} \alpha_{cb} K^T \left( \delta(c, \chi(z_i)) \right) d_{\beta_{cb}}(i) + J_{cb} \right) + I_c \right), \quad (\text{A.2})$$

with

$$d_{\beta_{cb}}(i) = \sum_{j=1}^{P_b} \beta_{cbj} (z_{ib}^j - w_{ib}^j)^2, \quad (\text{A.3})$$

where  $c$  indices the neurons of the 2S-SOM map.

under the two constraints:

$$\sum_{b=1}^B \alpha_{cb} = 1; \alpha_{cb} \in [0,1] \forall c, 1 \leq c \leq C \quad (\text{A.4})$$

and

$$\sum_{j=1}^{P_b} \beta_{cbj} = 1; \beta_{cbj} \in [0,1], \forall c, 1 \leq c \leq C; \forall b, 1 \leq b \leq B.$$

$I_c$  and  $J_{cb}$  are used to regularize the weights  $\alpha$  and  $\beta$ . They are defined as negative entropies weighted by  $\mu$  for the blocks and  $\eta$  for the variables of each block

$$I_c = \mu \sum_{b=1}^{P_b} \alpha_{cb} \log(\alpha_{cb}) \quad (\text{A.6})$$

and

$$J_{cb} = \eta \sum_{j=1}^B \beta_{cbj} \log(\beta_{cbj}) \quad (\text{A.7})$$

The topological conservation properties of 2S-SOM are influenced by the weights  $\alpha_{cb}$  and  $\beta_{cbj}$  in the classification through the hyper-parameters  $\mu$ ,  $\eta$  and the neighborhood parameter  $T$ .

The weights  $\alpha_{cb}$  and  $\beta_{cbj}$  respectively indicate the relative importance of blocks and variables in the neurons. Thus, the greater the weight of a block  $b$  or a variable  $j$ , the more the block or the variable contributes to the definition of the class (or neuron) in the sense that it makes it possible to reduce the variability of the observations in the cell and in its close neighborhood. For a high value of  $\eta$  and a fixed one for  $\mu$ , the  $\beta_{cbj}$  in a block are equal to  $1/P_b$ . In this case, only the blocks are modified according to their capacity to define the neurons. In this context, the 2S-SOM then makes possible to weight the different blocks for each neuron

- For high values of  $\mu$ ,  $I_c$  is large. The minimization of  $J_{cb}$  forces all its coefficients to become equal. For a fixed value of  $\eta$ , the  $\alpha_{cb}$  associated with the blocks are all equal to  $1/B$ . In this case, only the  $\beta_{cbj}$  of the variables inside the blocks weight the neurons
- When  $\mu$  and  $\eta$  tend to very large values, the blocks are equiprobable as well as the variables. Thus, the 2S-SOM algorithm is comparable to the SOM.

### **A.3 How the 2S-SOM algorithm works:**

For fixed  $\mu$  and  $\eta$ , the learning of the 2S-SOM algorithm is as follows:

- Step 0: Initialization with iteration of the algorithm SOM, by setting  $\alpha$  and  $\beta$  to homogeneous values.

The optimization of  $J_{2S-SOM}^T$  is carried out through an iterative process composed of three steps (1, 2, and 3) presented below.

- Step 1: The  $w_c$  referents, the weights  $\alpha$  and  $\beta$  are known and fixed, the observations are assigned to the neurons by respecting the assignment function:

$$c(z_i) = \chi(z_i) = \arg \min_{c \in C} \left( \sum_{r \in C} K^T(\delta(r, c)) \left( \sum_{b=1}^B \alpha_{cb} d_{\beta_{cb}}(i) \right) \right) \quad (A.8)$$

- Step 2: Updating the neuron centers (the  $w_c$  referents) according to the formula of the SOM algorithm.

- Step 3: the assignment function and the referents  $w_c$  being fixed,  $\alpha$  and  $\beta$  are determined according to the equations (A.9, A.10, A.11, A.12), by minimizing the cost function  $J_{2S-SOM}^T$  with respect to  $\alpha$  and  $\beta$  under the constraints A.4 and A.5.

$$\alpha_{cb} = \frac{\exp\left(\frac{-\psi_{cb}}{\mu}\right)}{\sum_{b=1}^B \exp\left(\frac{-\psi_{cb}}{\mu}\right)} \quad (A.9)$$

with

$$\psi_{cb} = \sum_{z_i \in D} K^T(\delta(\chi(z_i), c)) d_{\beta_{cb}}(i) \quad (A.10)$$

and

$$\beta_{cbj} = \frac{\exp\left(\frac{-\Phi_{cbj}}{\eta}\right)}{\sum_{b=1}^{p_b} \exp\left(\frac{-\Phi_{cbj}}{\eta}\right)} \quad (A..11)$$

with

$$\Phi_{cbj} = \sum_{zi \in D} \alpha_{cb} K^T(\chi(z_i), c) (z_{ib}^j - w_{cb}^j)^2 \quad (A.12)$$

This algorithm is repeated by sampling the hyper-parameters  $\mu$  and  $\eta$  until convergence.

Finally, at the convergence, the 2S-SOM provides on the one hand a topological map allowing to visualize the data, and on the other hand a weight system for the neurons of the map allowing us to interpret the role of the different variables and to choose those that are the most significant for the classification and neutralizing those which are the least one.

**FIGURE CAPTION**

Figure 1: *Mauritania and Senegal coastal topography. The land is in brown and the ocean depth is represented in meters by the color scale on the right side of the figure. The UPSEN stations are shown at the bottom left cartoon of the figure*

Figure 2: *Geographic positions of the 515 in situ and satellite collocated measurements of the DPIG database.*

Figure 3: *Dispersion diagram of DPIG chl-a computed from the SeaWiFS observations using the OC4V4 algorithm versus in situ chl-a. The coefficient of vraisemblance  $R^2$  and the RMSE (Root Mean Square Error) were computed in  $\text{mg m}^{-3}$*

Figure 4: *Flowchart of the method: top panel - Learning phase; bottom panel – operational phase which consists in pigment retrieval and the determination of the  $\alpha_{cb}$  block parameters.*

Figure 5: *Flowchart of the cross-validation procedure for 30 partitions of the DPIG database.*

Figure 6: *2S-SOM Map. From left to right and top to bottom, values of the referent vectors for  $\rho_w(490)$ ,  $Ra(490)$ , SeaWiFS chl-a, and fucoxanthin, peridinin, divinyl Ratios. The number in each neuron indicates the amount of DPIG data captured at the end of the learning phase, the values indicated by the color bars are centered-reduced and non-dimensional values.*

Figure 7: *2S-SOM map. Weights ( $\alpha_{cb}$ ) of the four block parameters determined at the end of the learning phase; from left to right and top to bottom:  $\rho_w$ ,  $Ra$ , Pigment, SeaWifs chl-a. The color bars show the % of the weight estimated by 2S-SOM, a value of 1 or 0 indicating that the data in the neuron are assembled with respect to that block only.*

Figure 8: *A) chl-a concentration, (B) fucoxanthin ratio, (C) aerosol optical thickness, (D) peridinin for 1 January 2003. Panels (B) and (D) show that a second-order information was retrieved, which is correlated with the chl-a concentration (A) but not equivalent. The aerosol optical thickness (C) does not seem to contaminate the estimated parameters (fucoxanthin and peridinin ratios).*

Figure 9: *SST for 2 January 2003. Note the well-marked upwelling (cold temperature) north of  $13^\circ\text{N}$ .*

1043  
1044  
1045  
1046  
1047  
1048  
1049  
1050  
1051  
1052  
1053  
1054  
1055  
1056  
1057  
1058  
1059  
1060  
1061  
1062  
1063  
1064  
1065  
1066  
1067  
1068  
1069  
1070  
1071  
1072  
1073  
1074  
1075  
1076  
1077

Figure 10: (A) *chl-a* concentration, (B) fucoxanthin ratio, (C) aerosol optical thickness, (D) peridinin for 6 January 2003. Panels (B) and (D) show that a second-order information was retrieved, which is correlated with the *chl-a* concentration (A) but is not equivalent. It is found that the aerosol optical thickness (C) does not contaminate the estimated parameters (fucoxanthin and peridinin ratios).

Figure 11: (A) *chl-a* concentration, (B) fucoxanthin ratio, (C) aerosol optical thickness, (D) Peridinin for 28 February 2003. Panels (B) and (D) show that a second order information was retrieved, which is correlated with the *chl-a* concentration (A) but is not equivalent. It is found that the aerosol optical thickness (C) does not contaminate the estimated parameters (fucoxanthin and peridinin ratios). The position of the NSB and OFB boxes are figured out by black square boxes

Figure 12: Reflectance spectra (in blue) captured the 28 February by six neurons whose referent vector spectra are in yellow: top line, for pixels in the NSB region (long.  $[-20^\circ, -18^\circ]$ , lat.  $[12^\circ, 14^\circ]$ ); bottom line, for pixels in the OFB region (long.  $[-28^\circ, -26^\circ]$ , lat.  $[12^\circ, 14^\circ]$ ).

Figure 13: Box plot of the weights of the selected neurons during the decoding of the 28 February data. From left to right, weights of blocks B1, B2, B3, B4. Top panel, in the NSB region (long.  $[-20^\circ, -18^\circ]$ , lat.  $[12^\circ, 14^\circ]$ ); bottom panel, in the OFB region (long.  $[-28^\circ, -26^\circ]$ , lat.  $[12^\circ, 14^\circ]$ ).

Figure 14: Monthly fucoxanthin concentration averaged for an 11- years (1998-2009) for December (A), March (B) and May (C).

Figure 15: . *chl-a* (in blue) and fucoxanthin (in green) concentrations for near-shore pixels (in the NSB region).

Figure 16: For ship stations 1, 2, 3, 5a and 5b, we show the averaged spectrum of the in situ spectra of the UPSEN station in blue; the spectrum of the referent vector (in red) of the 2S-SOM neuron, which has captured the closest satellite observations to the UPSEN station; among the different spectra constituting the referent spectrum, the spectrum of the learning database (DGIP) that is the closest to the averaged satellite spectra is shown in black. In the rectangular cartoons, we show the position of the UPSEN station, the number of the neuron of the 2S-SOM which has captured the satellite observation, the  $R_{\text{fuco}}$  of the referent vector, the  $R_{\text{fucoDGIP}}$  of the closest DGIP and the in situ  $R_{\text{fucoUPSEN}}$



1078

1079

1080 **Table Caption**

1081

1082 Table 1: *Pigments of the DPIG and their statistical characteristics: :STD (Standard Deviation), MIN*  
 1083 *(minimum value), MAX (maximum value).*

1084

1085 Table 2: *Statistical parameters ( $R^2$  coefficients, RMSE and P-values) of the cross validation between*  
 1086 *the DPIG in situ pigments and the pigments given by the 2S-SOM averaged for the 30 2S-SOM*  
 1087 *realizations*

1088

1089 Table 3: *For ship stations 1, 2, 3, 5a and 5b of the UPSEN campaigns, we show the referent captured*  
 1090 *by the VIIRS observations, the fucoxanthin-ratio associated with this referent (Rfuco-2S-SOM), the*  
 1091 *fucoxanthin-ratio of the closest DPIG fucoxanthin-ratio captured by the neuron of the referent and the*  
 1092 *fucoxanthin-ratio measured in situ during the UPSEN campaign*

1093

1094